Coordination Chemistry Reviews 255 (2011) 1085–1103

Contents lists available at ScienceDirect

Coordination Chemistry Reviews

journal homepage: www.elsevier.com/locate/ccr

Review

Theoretical studies on the reactivity of molybdenum enzymes

Sebastian Metz[a,*], Walter Thiel[b]

[a] Computational Science and Engineering Department, STFC Daresbury Laboratory, Daresbury, Warrington WA4 4AD, UK
[b] Max-Planck-Institut für Kohlenforschung, Kaiser-Wilhelm Platz 1, D-45470 Mülheim an der Ruhr, Germany

Contents

ARTICLE INFO

Article history:
Received 1 November 2010
Accepted 12 January 2011
Available online 31 January 2011

Keywords:
Molybdenum
Tungsten
DFT
QM/MM
Enzyme catalysis

ABSTRACT

In recent years, advances in theoretical methods and computational capabilities have made it possible to investigate reaction mechanisms in enzymes. Density functional theory (DFT) is commonly used to study reactions in model systems, while combined quantum mechanical/molecular mechanical (QM/MM) approaches allow the treatment of the complete solvated enzyme and thus provide insight into the mechanistic influence of the protein environment. This review starts with a brief overview over the available DFT and QM/MM methodology and then summarizes recent theoretical studies on biocatalysis by molybdenum-containing enzymes. It focuses on the reactions in members of the dimethylsulfoxide reductase, sulfite oxidase, and xanthine oxidase families, with special emphasis on the QM/MM studies of the latter. It concludes with a brief survey of theoretical work on some other molybdenum- and tungsten-containing enzymes.

1. Introduction

Experimental studies on enzymes and their reactivity continue to be challenging. Even with the whole arsenal of analytical tools at hand, it is often difficult to prove a proposed mechanism or to

* Corresponding author.
E-mail address: sebastian.metz@stfc.ac.uk (S. Metz).

0010-8545/$ – see front matter © 2011 Elsevier B.V. All rights reserved.
doi:10.1016/j.ccr.2011.01.027

characterize unstable intermediates with short life-times. Computational studies can be used to obtain a deeper understanding of enzymatic reactivity and to assist in the analysis of experimental results. Computational results may also be complementary and provide insights that cannot be obtained experimentally.

In this article, we review computational approaches to molybdenum-containing enzymes, focussing on reaction mechanisms and on how they are influenced by the protein environment. Most of the early computational studies on enzymatic reactivity were carried out with model systems, consisting of the cofactor (or a simplified model of it), the substrate, and in some cases also key active-site residues. Such studies often employ density functional theory (DFT). They may provide valuable understanding of the electronic structure of the reactive species, but the computed relative energies may strongly depend on the chosen model system and may not be transferable to the situation in the enzyme. In general, combined quantum mechanical/molecular mechanical (QM/MM) investigations are expected to provide more reliable results. They often consider reaction mechanisms proposed on the basis of previous gas-phase model calculations. Here, we will review both gas-phase QM model studies as well as QM/MM work. We will restrict ourselves to QM investigations that are directly related to the enzymatic reactions, and will not cover QM studies on inorganic model compounds.

This article is structured as follows: first, we give a short introduction to DFT and QM/MM methods (Section 2). We then present the computational results from the literature, ordered by enzyme families. We address in some detail dimethylsulfoxide reductases (Section 3), sulfide oxidases (Section 4), and xanthine oxidases (Section 5). For the latter family of enzymes, the available theoretical work is most extensive and includes four comprehensive QM/MM studies. Finally, we briefly survey theoretical studies on CO dehydrogenase and molybdenum-containing nitrogenases and give a short overview over the few investigations on tungsten-containing enzymes (Section 6).

2. Methods

2.1. DFT

Density functional theory is the most widely used method for modeling reaction mechanisms, especially when transition metals are involved [1,2]. Kohn–Sham DFT calculations employ a single determinant to represent the electron density, and they are thus similar in computational cost to ab initio Hartree–Fock (HF) calculations while being generally more accurate because of the inclusion of electron correlation via the exchange-correlation term [3,4]. However, there is no systematic way of improving DFT results, whereas the accuracy of ab initio results can be enhanced in a well-defined manner by using ever more refined explicit correlation treatments, such as second-order Møller–Plesset perturbation theory (MP2), configuration interaction (CI), or coupled cluster (CC) theory.

In practice, there is a large number of density functionals available to choose from. They can be categorized into local functionals (LDA, local density approximation), gradient-corrected functionals (GGA, generalized gradient approximation), meta-GGAs (GGAs with additional second-derivative correction terms), hybrid functionals (with some admixture of HF exchange, also called hyper-GGAs), and double hybrid functionals (with some admixture of MP2 correlation). While the accuracy and reliability of the DFT results generally tend to improve when moving towards the more refined functionals in this sequence, this cannot be taken for granted for any given molecular system, and careful validation is thus required in DFT studies to establish the appropriate functional for the planned specific application. The same applies to the choice of basis set.

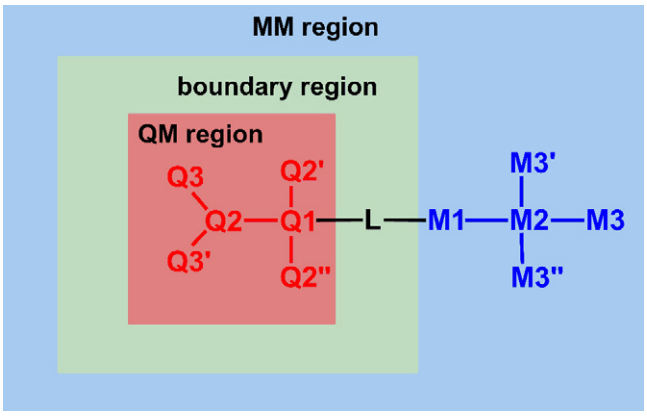

Fig. 1. QM/MM scheme and notation.

There is general consensus that DFT calculations with the established gradient-corrected functionals (e.g., BP86, BLYP or BPW91) and with moderate basis sets (e.g., of polarized double-zeta type) are sufficient to obtain reasonable optimized geometries. Hybrid functionals (e.g., B3LYP or B3PW91) are generally regarded more reliable for predicting relative energies, and they are therefore often employed in combination with larger (e.g., multiply polarized triple-zeta) basis sets in single-point calculations at GGA-optimized geometries. Especially the B3LYP functional has been shown to provide realistic results in a number of case studies [5–12].

Nowadays, systems with more than hundred atoms can be handled efficiently with DFT methods, and one may thus investigate rather large enzymatic model systems at a DFT-only level. However, most published DFT studies involve much smaller models and do not take the enzymatic environment into account. Starting geometries are usually taken from (possibly manually modified) crystal structures of the reactant or product complex, and geometry optimization techniques are then used to explore the potential energy surface and to find the relevant minima, transition states, and reaction paths. If these optimizations of gas-phase model systems are carried out without constraints (as is often the case), one may encounter an unnaturally large structural reorientation in the course of the reaction, which may not occur in the enzyme because of the steric constraints imposed by the protein environment. To avoid such artifacts one may fix certain (judiciously chosen) individual atoms at their position in the crystal structure and perform constrained optimizations. This is generally considered legitimate in spite of the bias that is introduced in this manner. Furthermore, it is common practice to mimic the effects of the neglected protein environment through a polarizable continuum with a properly chosen dielectric constant (which may be varied for sensitivity analysis). Such treatments (e.g., PCM or COSMO) are expected to capture environmental effects in an average manner. They should work better in neutral than in charged systems, but they may be problematic especially in systems with strong long-range electrostatic interactions (with concomitant active-site polarization).

2.2. QM/MM

In recent years, the hybrid QM/MM approach, originally introduced by Warshel and Levitt [13], has emerged as the method of choice for treating reactions in complex systems such as enzymes. Here, we only give a brief introduction, using the notation from Fig. 1, and refer the reader to recent reviews [14,15] for a detailed overview over QM/MM methods and their application to biomolecules.

The key idea of all QM/MM schemes is to divide a system of interest (that is too big to be completely treated by QM methods) into a QM part, where the reaction takes place, and a MM part, which accounts for the influence of the actual environment. Conceptually, the energy of such a QM/MM system can be obtained from subtractive and additive schemes, and the QM/MM interactions can be described by a variety of coupling schemes including mechanical, electrostatic, and polarized embedding. In addition, QM/MM methods may differ in the treatment of the QM/MM boundary, especially in cases when a chemical bond crosses the border between the QM and the MM region and thus needs to be cut. In this situation, all QM/MM studies reviewed here [16–23] use the link-atom approach [24] in which an unphysical atom or group L (normally a hydrogen atom) is added to saturate the valency of the QM frontier atom Q1 (see Fig. 1).

One of the most popular subtractive schemes is the ONIOM method [25–30] which has been applied to elucidate the reaction mechanisms of two members of the DMSO reductase family [16,17]. The energy function for such a scheme is given by Eq. (1), where Q, M, and L denote all QM, MM, and link atoms, respectively.

$$E_{\mathrm{QM/MM}}(\mathrm{Q,\,L,\,M}) = E_{\mathrm{MM}}(\mathrm{Q,\,M}) + E_{\mathrm{QM}}(\mathrm{Q,\,L}) - E_{\mathrm{MM}}(\mathrm{Q,\,L}) \quad (1)$$

E_{MM}(Q,M) is the MM energy of the complete physical system, i.e., comprising the atoms of the QM and the MM region (without link atoms). E_{QM}(Q,L) is the QM energy of the QM region including the link atoms. The double counting caused by adding E_{QM}(Q,L) is corrected by subtracting E_{MM}(Q,L), the MM energy of the QM region and the link atoms.

For additive schemes, the energy function is given by Eq. (2):

$$E_{\mathrm{QM/MM}}(\mathrm{Q,\,L,\,M}) = E_{\mathrm{MM}}(\mathrm{M}) + E_{\mathrm{QM}}(\mathrm{Q,\,L}) + E_{\mathrm{QM\text{-}MM}}(\mathrm{Q,\,M}) \quad (2)$$

Herein E_{MM}(M) is the MM energy for the MM atoms, excluding the atoms of the QM region and the link atoms. E_{QM}(Q,L) is again the QM energy of the QM region including the link atoms. The interaction between the QM and MM regions is represented by the third term $E_{\mathrm{QM–MM}}$(Q,M), which may differ between different QM/MM implementations. In all QM/MM studies reviewed here that employ an additive scheme [18–23], this term includes pair-wise non-bonded van der Waals and electrostatic interactions between the QM and the MM part. The van der Waals interactions are described by classical force-field expressions, with an attractive dispersion term and a repulsive term that captures steric effects and prevents clashes between oppositely charged atoms. The electrostatic interactions are included by incorporating the MM point charges into the QM Hamiltonian (electrostatic embedding).

Link atoms are positioned very close to the M1 point charge, which may lead to an overpolarization of the QM wavefunction. To minimize this problem, several correction procedures are available in the context of electrostatic embedding. Commonly employed [18–23] is the charge shift scheme [31,32] in which the charge from M1 is distributed evenly over the M2 atoms. The dipole created in this manner is compensated by a pair of point charges placed near each M2 atom, which generate dipoles of the same magnitude and opposite direction, such that the dipole moment along the M1–M2 bond vector reproduces the original dipole moment.

The setup for a QM/MM study of an entire enzyme is more complicated than the setup for a DFT model study. One normally starts from an experimental structure, for example, from a crystal structure deposited in the pdb database. However, in many cases, the available structural information is to some extent incomplete and may also include small errors or inconsistencies. Hence, one has to prepare a QM/MM setup which is normally done by following the procedures developed for classical MM simulations of proteins. Starting from a published crystal structure, this normally involves the replacement of an inhibitor molecule by the substrate, the addition of missing hydrogen atoms, the selection of protonation states for all pH active side chains, and possibly changes of the assigned orientation of side chains in ambiguous cases (e.g., His, Asn, and Gln). In addition, water molecules are normally placed in "empty" spots inside the enzyme and around the active site to realistically model a solvated enzyme. This is usually accomplished iteratively in a sequence of molecular dynamics (MD) simulations and energy minimizations, which are normally performed at the MM force-field level. From a final "production" MD run, several snapshots are taken and minimized, and the thus obtained geometries are used as starting structures for the QM/MM investigations.

QM/MM studies of enzymatic reactions normally employ geometry optimization techniques to find the reactions paths and the relevant minima and transition states on the potential energy surface. Because of the conformational complexity of enzymes, there may be many conformationally distinct pathways that contribute to the reaction (rather than a single one in typical gas-phase model studies), and it is thus important to do some sampling, at least at the level of investigating the reaction paths for several snapshots. A more complete sampling is computationally very demanding. In practice, free-energy calculations with proper sampling are feasible for semiempirical QM/MM methods (e.g., using thermodynamic integration or umbrella sampling), whereas DFT/MM free-energy calculations are often only practical in combination with approximate techniques such as simplified versions of free energy perturbation theory. For further information on these topics, the readers may consult recent QM/MM reviews [14,15].

Compared with QM/MM, DFT model studies have a simpler setup and involve less pitfalls, and they are simpler to execute. On the other hand, QM/MM studies provide a more complete and hence potentially more realistic picture of enzymes and the reactions being catalyzed, since they include the geometric constraints and the electrostatic influence of the protein environment in a natural manner. If properly performed, both approaches should lead to analogous results. Due to the explicit incorporation of the MM environment, the QM/MM results should converge faster with regard to the size of the QM region [33], and they can be analyzed rather easily, e.g., concerning the effects of specific residues. In many respects, DFT and QM/MM studies on enzymatic reactions are complementary to each other, and they are thus expected to coexist for quite some time to come.

3. The dimethylsulfoxide reductase family

3.1. Nitrate reductase

Nitrate reductase is a crucial enzyme in the biological nitrogen cycle, catalyzing the conversion of nitrate to nitrite. The first investigations on the enzymatic reaction mechanism [16,34] reported DFT calculations for model systems as well as QM/MM (ONIOM) calculations, with focus on the N–O bond breaking step. Starting from the crystal structure available at that time, they supported the mechanism that had previously been deduced experimentally (see Fig. 2). This mechanism was later refined [35] by taking into account a water molecule as sixth ligand at the central molybdenum atom as well as several naturally occurring modifications of the original cystein ligand. These studies suggested a first coordination sphere mechanism, i.e., a direct interaction between a nitrate oxygen atom and the molybdenum center (see Fig. 2). This was further supported by calculations on structurally similar model systems that dealt with a reverse reductive reaction [36].

However, revision of the crystal structure led to a different cofactor, bearing one more sulfur atom. In addition, experimental evidence from spectropotentiometry indicated that nitrate binding to the active side probably involves only Mo(V) or Mo(VI) rather than Mo(IV) species. Calculations using the new cofactor structure were reported by Hoffman [37], Cerqueira et al. [38] and Xie and Cao

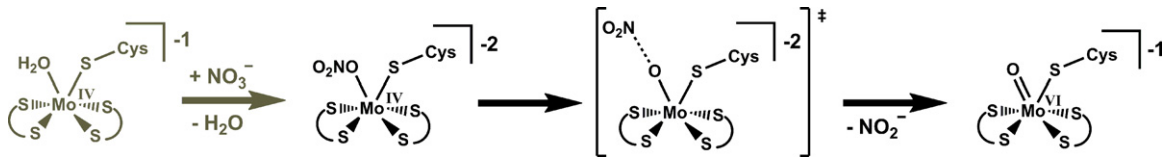

Fig. 2. Initially proposed reaction sequence for nitrate reductase [16,35]; the grey-colored part was investigated only in the later study [35].

[39]. The investigated mechanisms can be categorized into inner coordination sphere mechanisms (A and B) and outer coordination sphere mechanisms with molybdenum in the Mo(VI) (C) or Mo(V) state (D). In Fig. 3 these four proposals are shown in one single scheme (with some modification of the notation used in the original publications).

In the two inner-sphere mechanisms (ISM), nitrate is a ligand of the central molybdenum atom in the initially formed complex. In ISM-A, one of the Mo–S interactions is replaced by a Mo–O interaction, whereas in ISM-B, the coordination number of the central molybdenum atom is increased from 6 to 7 to bind the nitrate as an extra ligand. In both cases, the N–O bond is then broken, and nitrite is released. The reported barriers for ISM-A vary strongly, between 15.3 [39] and 20.2 [38] kcal mol^{-1} up to more than 40 kcal mol^{-1} [37]. By comparison, ISM-B has a rather low barrier of 12.6 kcal mol^{-1} [39] and thus seems to be the preferred inner-sphere mechanism. The two outer-sphere mechanisms (OSM) differ in the electronic state of the molybdenum center. The reported barriers for the O_2NO–S bond formation (i.e., the first step) are exceedingly high (56.8 kcal mol^{-1} for OSM-C [39] and 50.6 kcal mol^{-1} for OSM-D [38]), and hence these mechanisms can safely be excluded from being catalytically active. Judging from these results, ISM-B appears to be the most likely mechanism. One should note, however, that none of the atoms belonging to the dithiolene ligand were restrained in these model calculations so that the penalty of increasing the Mo coordination number from 6 to 7 may be underestimated.

For ISM-A and OSM-D, further calculations addressed the O–NO_2 bond breaking step and the question of how electrons and protons are subsequently added to convert the formed oxo ligand (see Fig. 3) into a water molecule which then needs to be released to close the catalytic cycle. Details can be found in the original publications [37,38].

3.2. Dimethylsulfoxide reductase

DMSO reductase is the prototype of this enzyme family. It catalyzes oxygen atom transfer reactions, in particular the conversion of dimethylsulfoxide (DMSO) to dimethylsulfide (DMS). This reaction was first studied with DFT(B3LYP) gas-phase model calculations by Webster and Hall [40], see Fig. 4. They reported a reaction barrier of 8.9 kcal mol^{-1}, and the corresponding transition state for

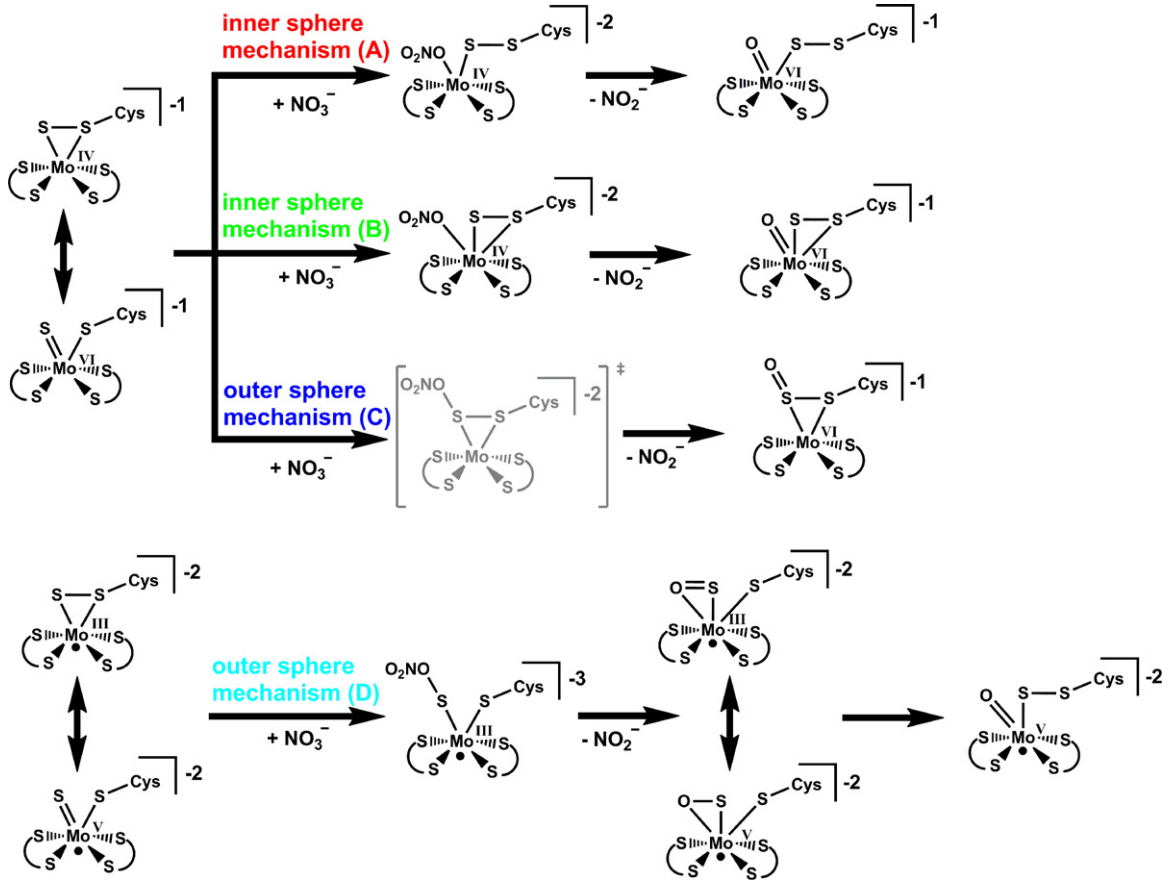

Fig. 3. Four reaction mechanisms for nitrate reductase: two inner-sphere mechanisms with direct Mo–ONO_2 interaction (A and B) and two outer-sphere mechanisms with S–ONO_2 interaction and a total charge of −1 (C) and or −2 (D). The grey color of the transition state in mechanism C indicates that it involves S–O bond formation with concomitant product release.

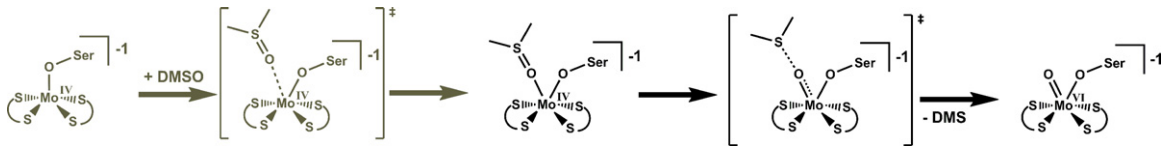

Fig. 4. Reaction mechanism of DMSO reductase. The black-colored structures show the sequence studied by Webster and Hall [40]. The first part was later reported by Thapper et al. [46] using a slightly different model for the cofactor, and later confirmed by McNamara et al. [47,48].

S–O bond breakage was geometrically very similar to the minimum structure of the reactant complex in the enzymatic environment. Constraining the dithiolene ligands destabilized the reactant much less (1 kcal mol^{-1}) than the product (8 kcal mol^{-1}). The role of the enzyme was therefore claimed to maintain the active site structurally similar to the transition state. This would then minimize the reorganization energy (entatic principle [41,42]) and reduce the exothermicity of the reaction, thus generating a thermodynamic sink. Mohr et al. [17] confirmed the computed gas-phase barrier height (8.8 kcal mol^{-1}, again by B3LYP) and reported a considerably reduced QM/MM (ONIOM) barrier of 4.6 kcal mol (using the semiempirical PM3 method as QM component). This QM/MM value seems too low in view of kinetic data from model complexes [43] and enzymatic experiments [44,45], suggesting that either the PM3 approach is not accurate enough or that the rate-determining barrier was not properly identified.

Thapper et al. indeed showed that it is not sufficient to consider only S–O bond cleavage, since substrate association is an endothermic process which must be taken into account to obtain the correct overall barrier [46]. They obtained a value of 14.6 kcal mol^{-1} (between the reactant and TS2) using a slightly different model system, which however conserved the general geometrical features found previously, in particular the trigonal-prismatic geometry of the rate-limiting transition state. The electronic factors that lead to a preference of a trigonal-prismatic over an octahedral structure were analyzed in detail by Kaupp [49]. The findings of Thapper et al. [46] were later confirmed for the original model system by McNamara et al. [47,48] and by Hernandez-Marin and Ziegler [50], who obtained a barrier (again between the reactant and TS2) of 19.2 kcal mol^{-1} [47,48] and 16.6 kcal mol^{-1} [50], respectively. The two-step mechanism depicted in Fig. 4 seems to be commonly accepted by now, leaving the precise individual barrier heights as a continuing topic of discussion. In a systematic study, Hofmann [51] applied a broad variety of ab initio methods (MP, CI, and CC) and density functionals, and he was able to demonstrate that the DFT methods, and especially the B3LYP functional, perform quite well for this reaction. Finally, unlike the case of ethylbenzene dehydrogenase (see below), it was shown that the reactive species in DMSO reductase are essentially of closed-shell type, without any appreciable radical character [52].

3.3. Ethylbenzene dehydrogenase

Ethylbenzene dehydrogenase (EBDH) is a key biocatalyst in the metabolism of ethylbenzene-degrading bacteria such as *Aromatoleum aromaticum*. It catalyzes the stereospecific hydroxylation of ethylbenzene to (*S*)-1-phenylethanol [53]. Following up on suggestions from an experimental paper [53] three reaction mechanisms were considered [54]: a radical mechanism with an Mo(V) intermediate (I_r), a mechanism initiated by a hydride transfer leading to a Mo(IV) intermediate (I_h), and a combination of these two mechanisms which can be connected by an electron transfer reaction, see Fig. 5. To distinguish between these different mechanisms for ethylbenzene oxidation, DFT calculations on model systems of different size derived from the EBDH crystal structure [55] were performed and combined with kinetic isotope experiments to elucidate the reaction mechanism and to determine whether the reaction proceeds via one two-electron or two one-electron transfers. Further topics were the influence of His192 and its protonation state on the reaction and the consequences of different possible arrangements of the molybdopterin ligand. According to these investigations, EBDH is one of the few cases where the oxygen transfer step proceeds via a radical mechanism, which has a lower energy barrier than the corresponding two-electron transfer mechanisms. The

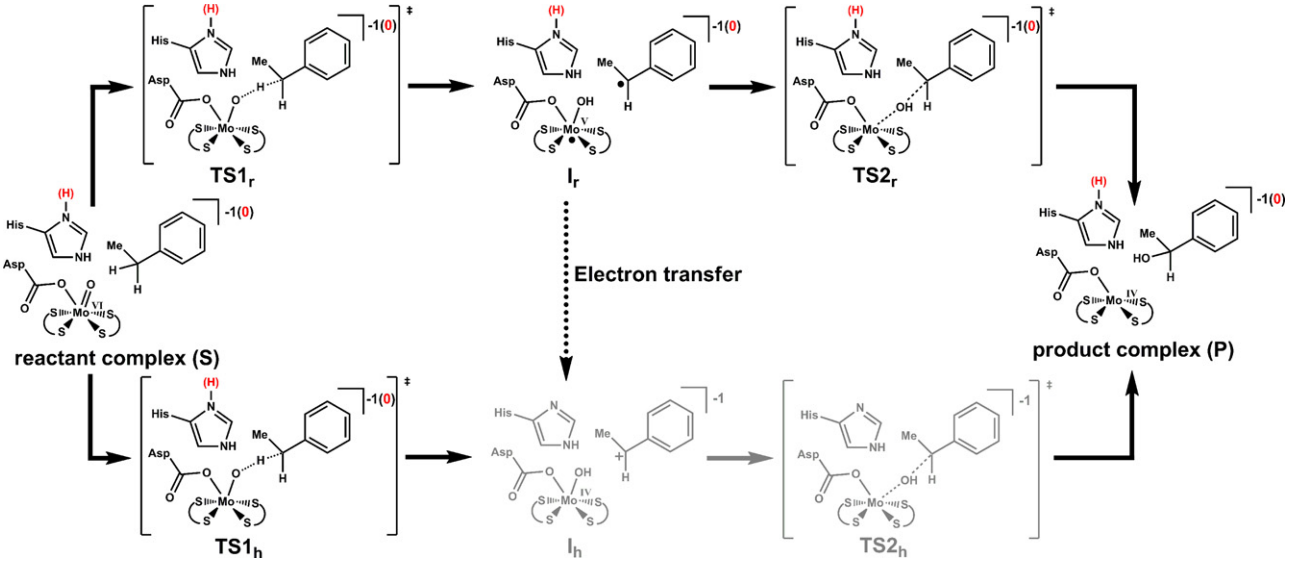

Fig. 5. Mechanisms for EBDH considered by Szaleniec et al. [56]. (a) Radical mechanism (top): the same pathway was found for both protonation states of histidine (with different barriers). (b) For the hydride transfer initiated mechanism (bottom), I_h and $TS2_h$ (grey) could only be located for deprotonated histidine. For protonated histidine, $TS1_h$ collapsed immediately to the product complex (P).

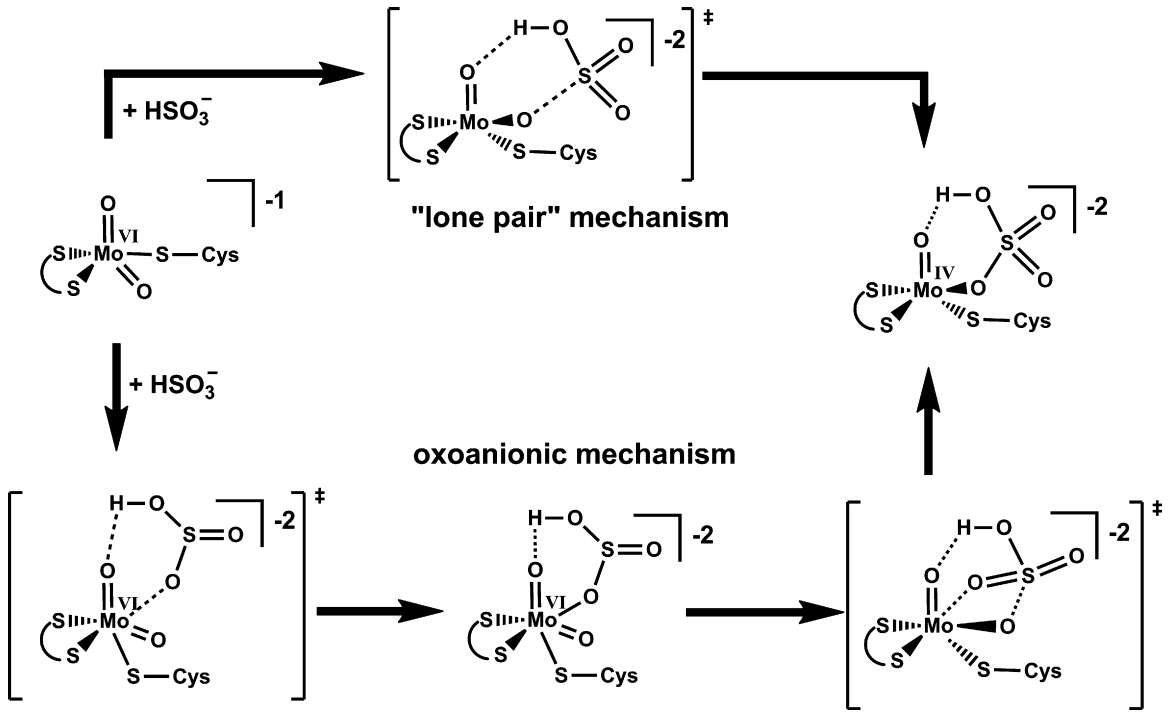

Fig. 6. Alternative reaction mechanisms of sulfite oxidase acting on hydrogen sulfite [57].

preferred pathway involves two transition states, see Fig. 5: $TS1_r$ associated with C–H bond cleavage, and the carbocation-type $TS2_r$ associated with the transfer of the second electron and OH rebound. These findings were independent of the actual protonation state of His192. Qualitative agreement was reached between the kinetic isotope effects calculated for $TS1_r$ and measured experimentally at optimum pH.

4. The sulfite oxidase family

4.1. Sulfite oxidase

Sulfite oxidase (SO) is a hepatic molybdenum-containing enzyme in charge of detoxification and oxidative degradation of sulfur-containing amino acids. SO deficiency may lead to neurological problems or dislocation of the ocular lens. The first investigation closely related to the reaction mechanism of sulfite oxidase was performed by Thapper et al. [36], who presented a two-step pathway for the conversion of hydrogen sulfite to hydrogen sulfate, with initial S–O bond formation followed by Mo–O bond cleavage. However, they used a gas-phase model system derived from DMSO reductase so that the computed energetics are unlikely to be representative of the enzymatic reaction in SO. In the first explicit computational study of this reaction [57], Pal et al. investigated two distinct reaction mechanisms, a "lone pair" and an oxoanion mechanism, see Fig. 6:

The "lone pair" mechanism assumes a direct reduction of the Mo(IV) center by the lone pair of the hydrogen sulfite, with concomitant S–O bond formation and without extension of the coordination sphere. This one-step mechanism was computed to have a much higher barrier than the formation of the intermediate in the oxoanion attack and was therefore dismissed also for the enzyme [57].

In the alternative oxoanion mechanism, the hydrogen sulfite substrate first coordinates via one of its oxygen atoms to the molybdenum center, increasing the coordination number from 5 to 6. This is followed by S–O bond formation which reestablishes the five-coordinated cofactor. This second step was calculated to be rate-determining. However, the reported barriers [57] for the oxyanion mechanism were about 67 kcal mol^{-1} for gas-phase models and about 30–32 kcal mol^{-1} for continuum solvent models, much higher than the experimental value of about 12 kcal mol^{-1} [58].

In a more recent study of this reaction, Hernandez-Marin and Ziegler used sulfite (instead of hydrogen sulfite) as substrate and included methyl guanidinium to model the Arg138 side chain and to keep the cofactor site neutral [59]. They calculated a reaction sequence similar to the "lone-pair" mechanism investigated by Pal et al. [57] and also considered product release, see Fig. 7. The latter step was rate-limiting, with an activation free energy (BP86, COSMO, $\varepsilon = 5$) of $\Delta G(298\,K) = 14.5$ kcal mol^{-1}, which is quite close to the experimental value. The alternative mechanism, in which the sulfite first coordinates to the molybdenum, was not studied in this work [59].

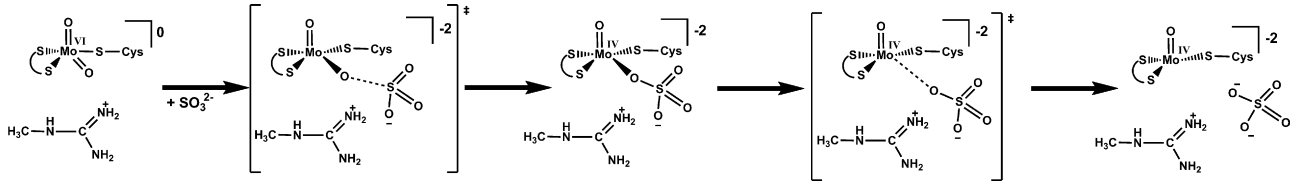

Fig. 7. Reaction mechanism of sulfite oxidase acting on sulfite [59].

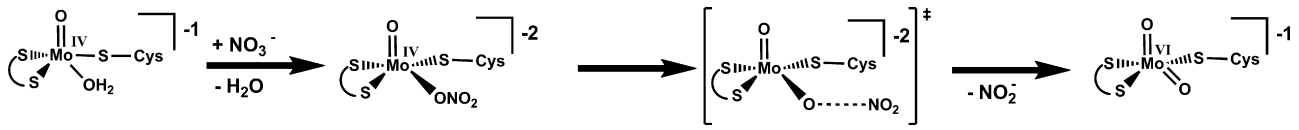

Fig. 8. Reaction mechanism for a model of assimilatory nitrate reductase [35]: the exchange of water by nitrate is followed by N–O bond cleavage and product release.

4.2. Nitrate reductase

There are several theoretical studies on nitrate reductase enzymes assigned to the DMSO reductase family, but only one on the assimilatory nitrate reductase that belongs to the sulfite oxidase family [35]. Based on the thermochemistry of the exchange reaction with nitrate, the initial five-coordinated molybdenum complex was assumed to contain a water ligand, rather than a hydroxy ligand, see Fig. 8. In B3LYP and B98 calculations, the exchange of this water molecule by nitrate was exothermic (no transition state reported), and the subsequent O–N bond cleavage was the rate-determining step, with a barrier of about 12–15 kcal mol^{-1}. Mechanistically, one therefore obtains the reverse of the reaction catalyzed by sulfite oxidase.

5. The xanthine oxidase family

Compared with the previously discussed enzyme families, the structure of the cofactor and the reaction mechanisms are more controversial for the enzymes from the xanthine oxidase (XO) family. To set the stage for the presentation of the theoretical results, we first briefly summarize the available experimental information on the cofactor and the reactivity of these enzymes.

5.1. The cofactor

The molybdenum-containing enzymes can be classified on the basis of their cofactors. The molybdopterin cofactor defining the xanthine oxidase family is shown in Fig. 9. In different members of this family, it may differ in its nucleotide part and may therefore interact differently with the corresponding apoenzymes. A detailed analysis of these interactions for the cytidine (cytosine + ribose) monophosphate molybdopterin cofactor within aldehyde oxidoreductase (AOR) was published by Romão et al. [60]. Apart from this form, guanosine (guanine + ribose) monophosphate, adenosine (adenine + ribose) monophosphate, and inosine (hyperxanthine + ribose) monophosphate variants were identified [61].

The exact coordination of the central molybdenum atom has been controversial for quite some time, and various possible coordination patterns have been explored computationally [62–64]. Based on these theoretical results and on various EXAFS experiments [65–70], the central atom of the molybdopterin cofactor in XO has been assigned to carry two thiolate ligands (S–Mo) from the connection to the pterin subunit, one terminal oxo ligand (Mo=O_{ap}), one hydroxy ligand (Mo–OH), and one terminal sulfido ligand (Mo=S_{eq}) [63]. This assignment has been confirmed by more recent experimental data [71]. It is now generally accepted as common structural feature within the xanthine oxidase family [72–74] and has been used in nearly all theoretical investigations on this topic [63,75–81]. However, in the first crystal structure published for AOR, the hydride acceptor ligand in the equatorial plane (X_{eq}, see Fig. 9) was reported to be an oxygen atom (O_{eq}) [82]. As the analogous desulfo form of XO was known to be inactive [83], it was assumed that this crystal structure of AOR may represent an inactive variant of the naturally active sulfido form. Attempts to restore activity by resulfuration with H_2S failed as the sulfur atom was added to the apical position (S_{ap}) while the equatorial position was still occupied by an oxygen atom, O_{eq}. However, it was recently suggested that AOR may also work with an equatorial oxo ligand, as a variant of the commonly accepted sulfido form [84].

In view of the continuing discussion about the nature of the X_{eq} ligand in the molybdopterin cofactor, detailed QM/MM investigations with X_{eq} = O, S, and Se were performed for the experimentally well studied case of XO [22] and the presumably analogous AOR system [19,23]. They strongly suggest that the active cofactor of both AOR and XO should carry a sulfido ligand (X_{eq} = S). The exchange of S against Se slightly reduces the rate-limiting barrier, consistent with the presence of Se in the cofactor of the related nicotinate dehydrogenase enzyme [85]. By contrast, the substitution of S by O raises the rate-limiting barrier for both enzymes significantly and makes them inactive (for further details see Sections 5.4 and 5.5).

5.2. The catalytic cycle

The molybdenum-containing cofactor of xanthine oxidase catalyzes the conversion of xanthine to uric acid. Two different mechanisms have been proposed for this reaction, as shown in Fig. 10. In the first one (light blue), a direct interaction between the substrate nitrogen atom and the central molybdenum atom (B) is assumed [86] prior to the concerted formation of an Mo–C bond and the transfer of a hydrogen atom to the sulfido group (in C). The activated substrate can then be attacked by a hydroxy group either from a deprotonated water molecule or from a hydroxy group attached to molybdenum prior to formation of the carbon-bound tetrahedral intermediate (D). This species is reduced to an Mo(IV) intermediate (E). By transferring one electron from molybdenum via the iron–sulfur cluster to the FAD cofactor and the loss of one proton, the presumedly ESR-active intermediate (F) is formed. In this context, a more pronounced Mo–C or Mo–O interaction is claimed

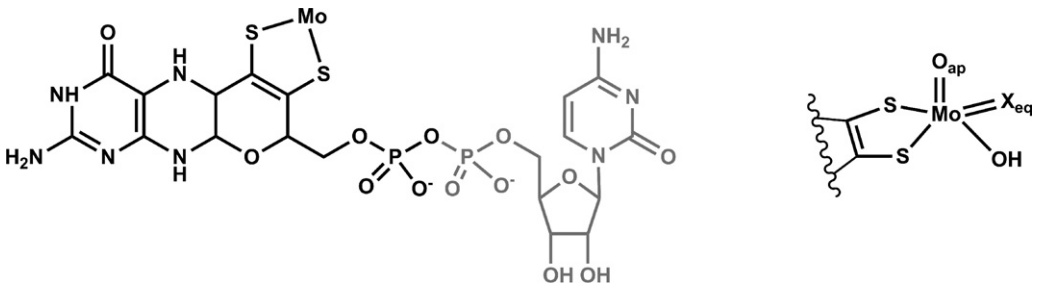

Fig. 9. Cytidine monophosphate molypdopterin cofactor in AOR. The nucleotide part drawn in grey may differ in other cofactor species, see text.

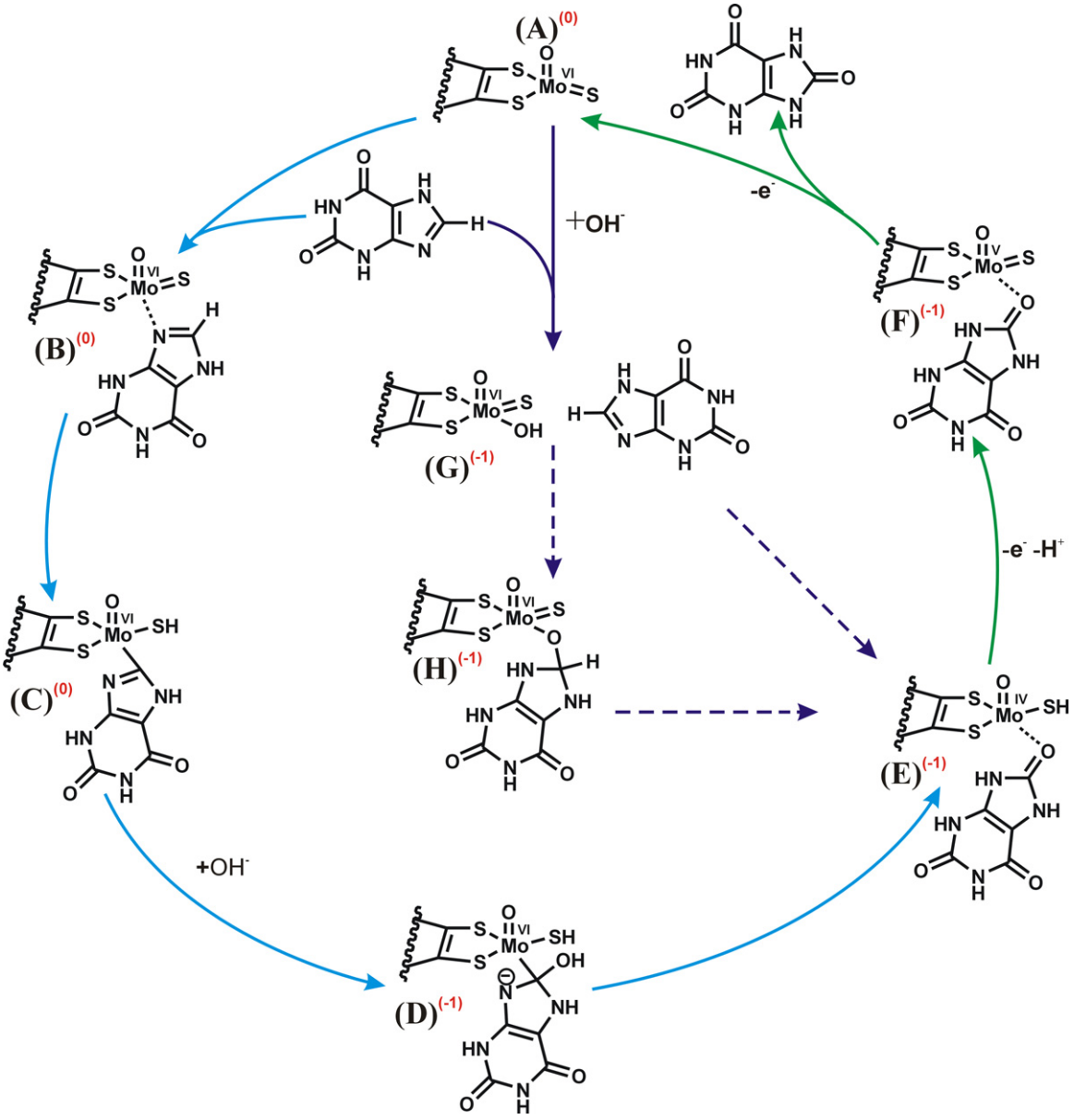

Fig. 10. Reductive half-cycle of XO with different suggested pathways, see text. One particular representation of possible protonation states and substrate orientations was selected for this figure. The overall charge of the depicted species is given in parentheses, colored in red.

[86,87]. A significant Mo–C interaction is supported by recent X-ray data, which show a similar coordination of an ethylene glycol and glycerol inhibitor in AOR [84].

The second pathway (dark purple) is favored in the recent literature [87–91], but remains controversial in its details. Herein, the active form of the cofactor bears the catalytically active hydroxy group attacking the substrate (G). One open question is whether the reaction follows a one-step mechanism to form the product-bound form (E) or whether it proceeds via a tetrahedral intermediate (H). Further issues are the orientation of the substrate within the binding pocket and the actual tautomer of the xanthine substrate that undergoes the reaction.

5.3. DFT studies

The first model study on the reaction mechanism in XO was performed at the B3LYP/Lanl2DZ level in 1997 [63]. It addressed the oxidation of an aldehyde by a simplified cofactor species (see Fig. 11). In the first step of the suggested mechanism, the substrate transfers its hydrogen atom to the sulfido group while binding to molybdenum. In the second step, there is a nucleophilic attack of the cofactor hydroxy group on the carbonyl group of the substrate that leads to C–O bond formation and Mo(VI) → Mo(IV) reduction. The transition state for the first step was not located, while the barrier for the second step was reported to be 8.4 kcal mol^{-1}. As in

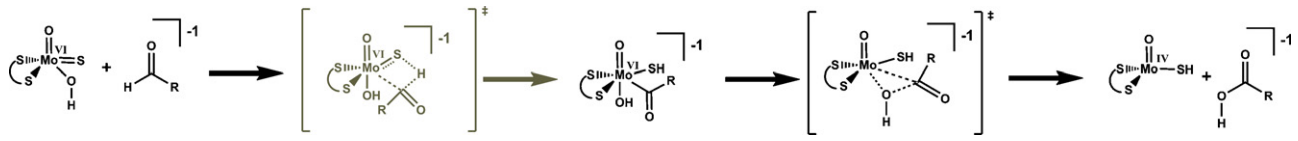

Fig. 11. Reaction sequence reported by Bray and Deeth [63]. The grey-colored transition state was not located.

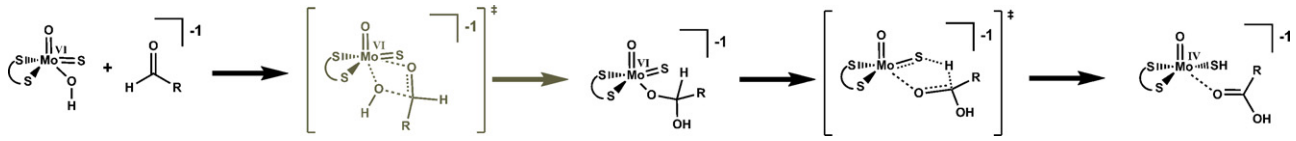

Fig. 12. Reaction sequence reported by Voityuk et al. [76]. The grey-colored transition state was not located.

the light-blue colored pathway in Fig. 10, a direct Mo–C interaction was assumed in this pathway.

The pathways colored in dark purple in Fig. 10 do not involve any direct Mo–C interaction, retaining the original coordination number of five. This can be achieved by either a stepwise or a one-step mechanism. The former was addressed by Voityuk et al. [76] who proposed a two-step reaction with formation of a tetrahedral intermediate and subsequent hydride transfer (using the BP86 functional). However, barriers were only reported for the hydride transfer step, not for the initial formation of the tetrahedral intermediate, see Fig. 12.

The one-step mechanism (Fig. 13) was first considered by Ilich and Hille [77], but due to the chosen level of theory (UMP2), the computed barrier was much too high and not comparable to the previous results. The most complete model study at the DFT(B3LYP) level was reported by Zhang and Wu [78] who gave a direct comparison between the concerted mechanism and the stepwise pathway via a tetrahedral intermediate (see Fig. 13) using formaldehyde as substrate. Their computed barriers were 11.9 kcal mol^{-1} for the concerted pathway, and 17.8 and 5.4 kcal mol^{-1} for the stepwise mechanism.

Barriers from highly correlated ab initio calculations were reported by Amano et al. [79] using the less active formamide as substrate and assuming a deprotonated cofactor. However, the computed overall barriers of 35–42 kcal mol^{-1} were prohibitively high. The only mechanistic study using xanthine as substrate suggested a concerted mechanism [81], but without considering a stepwise mechanism.

All these QM model calculations are limited in scope. They suffer, for instance, from incompleteness of the calculated reaction paths [63,76], from unrealistically high barriers [77,79], or from mechanistic steps that are not compatible with the available experimental results [92]. Moreover, all these investigations employ QM model systems that consist of only part of the cofactor and a (model) substrate. They do not include the active-site residues, and therefore cannot account for the steric and electronic influence of the enzymatic environment which proves to be of crucial importance, as shown in subsequent QM/MM work.

5.4. QM/MM investigations for aldehyde oxidoreductase

The first QM/MM study [19] on the mechanism of the reductive half-reaction of AOR (i.e., the conversion of an aldehyde to the corresponding acid) explored five possible pathways for the oxidation of acetaldehyde, taking into account different approaches of the substrate and the catalytic effect of the nearby glutamic acid (Glu869). One setup involved protonated Glu869 which precludes the activation of the cofactor by Glu869 acting as a Lewis base and thus results in a prohibitively high effective barrier, so that this pathway could be discarded. For the setup with deprotonated Glu869, three distinct pathways were found, see Fig. 14. A variant of the Lewis base catalyzed mechanism was considered by including one additional water molecule between Glu869 and acetaldehyde in an enlarged QM region, on the grounds that this water molecule may help to position the substrate and act as oxygen source for the next turnover. However, this variant did not improve the energetics (compared to the system without the extra water molecule), and will thus not be discussed further.

Each of the remaining three pathways (Fig. 14) involves three elementary transformations: the hydrogen atom of the

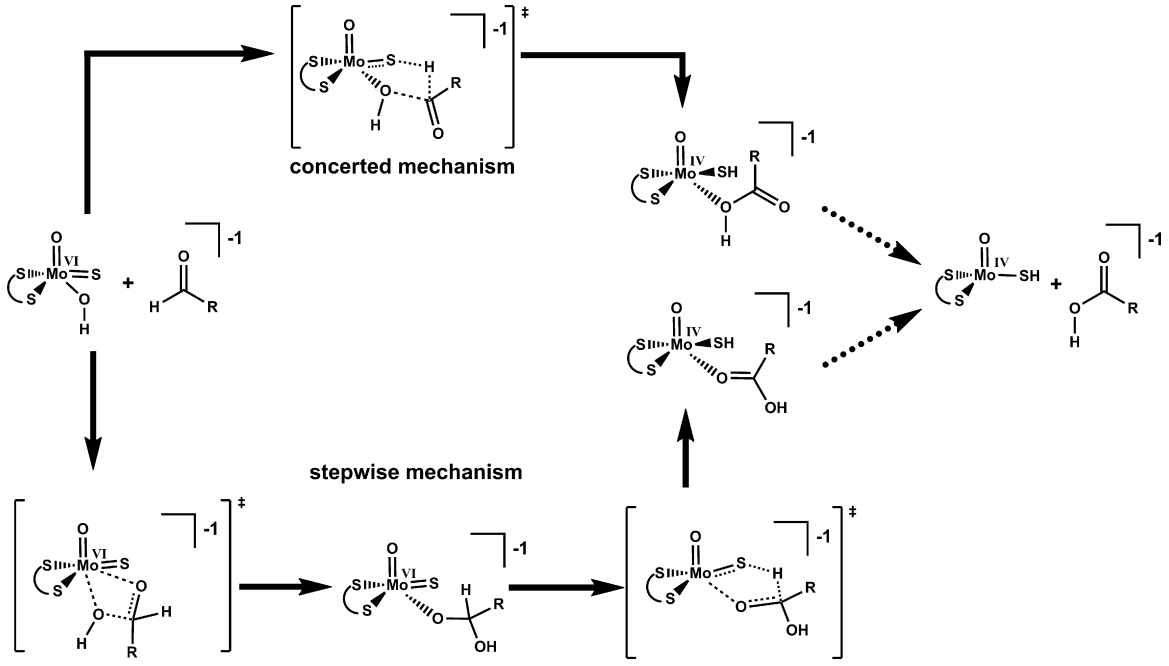

Fig. 13. Mechanisms considered in QM model studies for XO enzymes. (a) Protonated cofactor: concerted and stepwise pathways reaction sequences were reported [76–78]. (b) Deprotonated cofactor (without proton shown in red): only a concerted and no stepwise mechanism was found [79].

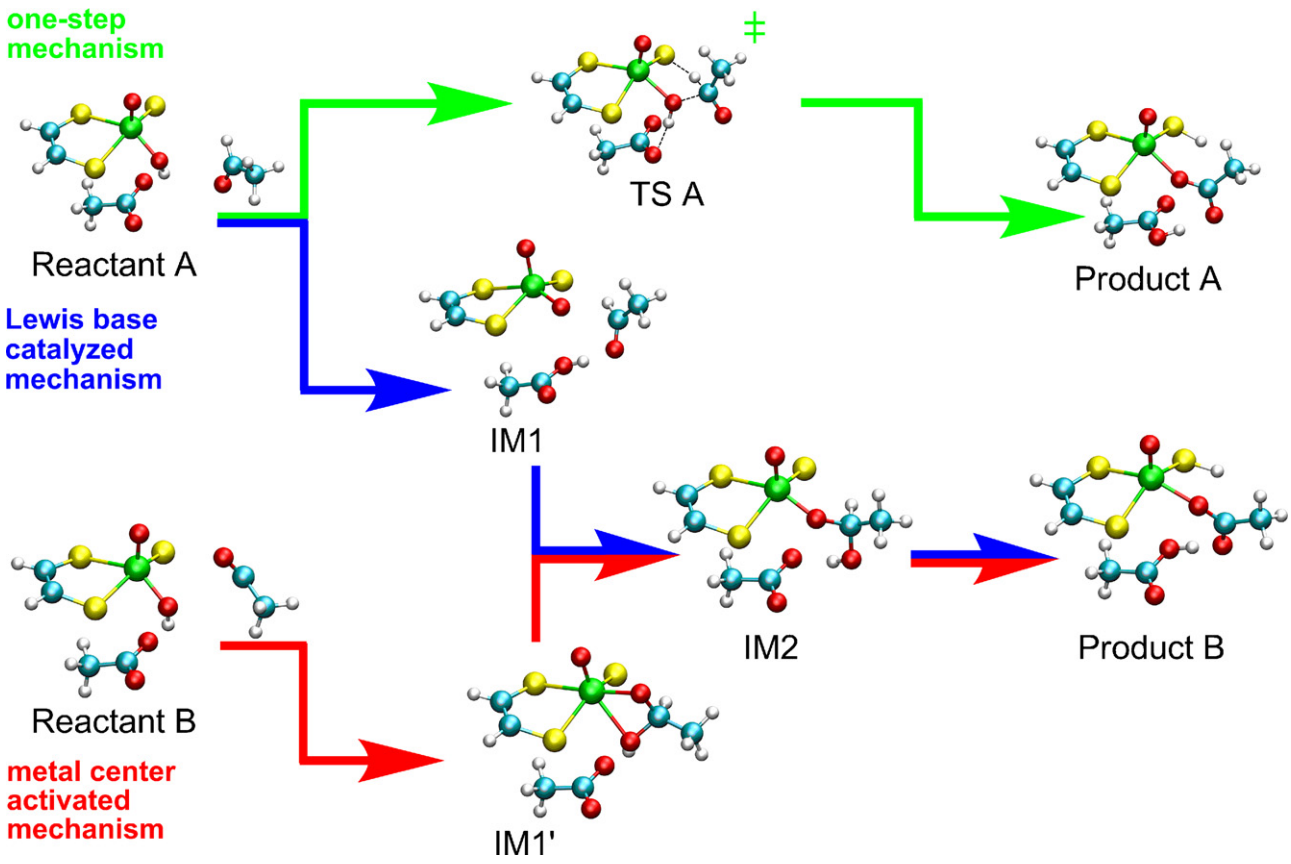

Fig. 14. Three competing reaction mechanisms for the oxidation of acetaldehyde by AOR. Reproduced from Ref. [21], with permission of the copyright holders.

molybdenum-bound hydroxy group is transferred to Glu869, a bond is formed between the equatorial oxygen atom and the carbon atom of the substrate carbonyl group, and a hydrogen atom is transferred from this carbon atom to the equatorial sulfido ligand.

In the one-step mechanism, the reaction proceeds through a five-membered transition state, see Fig. 14. Because of steric constraints, this one-step pathway is not accessible to bulkier substrates such as benzaldehyde (see below). The nearby Glu869 is essentially a spectator residue and does not promote the reaction significantly, but it does stabilize the product complex.

In the Lewis base activated mechanism, Glu869 participates actively in the mechanism and deprotonates the hydroxide group of the cofactor to form a first intermediate (IM1), see Fig. 14. This proton transfer is essential for the high activity of the enzyme towards the substrate, for two reasons: first, the oxygen atom of the former hydroxy group becomes more nucleophilic. Second, the newly formed H-bond from the proton at Glu869 perturbs the carbonyl group of the substrate and induces an electron flow to the carbonyl oxygen atom, which enhances the electrophilicity of the target carbon atom in the substrate. In the next step, the thus activated cofactor and the substrate form a C–O bond yielding a tetrahedral intermediate (IM2). According to the QM/MM data, the catalytic effect of Glu869 mainly lowers the barrier of this nucleophilic attack so that the subsequent formal hydride transfer becomes the rate-determining step in the reductive half-reaction. More precisely, this final step is actually a coupled proton-hydride transfer in AOR.

The metal center activated mechanism reaches the tetrahedral intermediate IM2 on a different route: the substrate first forms a C–O bond by coordinating its carbonyl group to the metal center and at the same time forming a bidentate complex (IM1′), which then rearranges to IM2. The final step is the same as in the Lewis base catalyzed mechanism.

The DFT(B3LYP)/MM calculations with acetaldehyde as substrate identify the Lewis base catalyzed mechanism as the favored one. The rate-limiting barrier is only 8.5 kcal mol^{-1} (for the final step), compared with 20.2 and 15.4 kcal mol^{-1} for the one-step and the metal center activated pathways, respectively. The crucial difference is the active involvement of Glu869 which acts as a Lewis base and activates the cofactor by an initial proton transfer.

An analogous mechanism was found for benzaldehyde as substrate [23]. In this case, no pathway other than the Lewis base catalyzed mechanism could be located. The only minor difference from the acetaldehyde case is that the deprotonation of the cofactor and the formation of a hydrogen bond to the substrate are now two distinct steps, see Fig. 15; all other steps are completely analogous. The QM/MM relative energies for the Lewis base activated pathways of benzaldehyde are given together with those of acetaldehyde in Table 1.

Table 1
QM(B3LYP/B1[a])/MM relative energies of the Lewis base catalyzed mechanism in AOR, for the substrates acetaldehyde and benzaldehyde, in kcal mol^{-1}. Barriers relative to the preceding minimum are given in parentheses.

	Acetaldehyde		Benzaldehyde	
Reactant	0.0		0.0	
TS1	4.6	(4.6)	5.8	(5.8)
IM1	−1.7		1.8	
TS1′			2.4	(0.6)
IM1′			−0.1	
TS2	4.9	(6.6)	6.0	(5.9)
IM2	−5.6		−0.3	
TS3	2.1	(7.7)	6.9	(7.2)
Product	−19.0		−19.6	

[a] B1 denotes a combination of the 6-31G* basis set for H, C, N and O [93,94] and a modified Lanl2DZ basis set for S [95,96] and Mo [97,98].

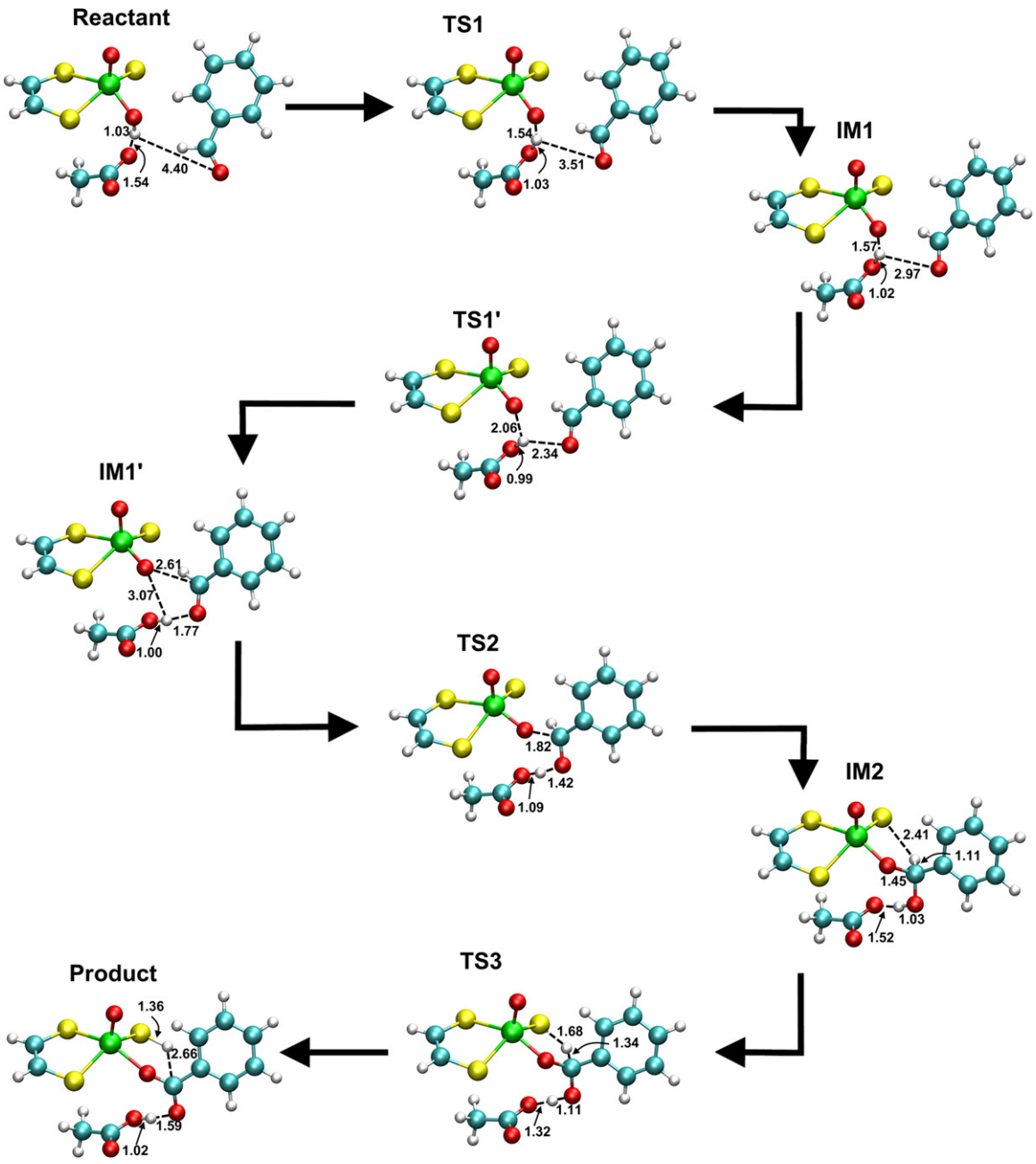

Fig. 15. Reaction mechanism of AOR with benzaldehyde as substrate. In the first two steps, the cofactor is deprotonated, and a new hydrogen bond is established to the substrate. Thereafter, a C–O bond is formed and a formal hydride transfer (coupled with a proton transfer) leads to the product.

Comparison of the data in Table 1 shows that the actual deprotonation step (TS1) has similar barriers for the two substrates (4.6 vs. 5.8 kcal mol^{-1}). The additional barrier (TS1′) in the case of benzaldehyde is very low (0.6 kcal mol^{-1}) and does not affect the general shape of the energy profile. The nucleophilic attack is slightly less facile for acetaldehyde (6.6 vs. 5.9 kcal mol^{-1}), as is the final hydride transfer (8.5 vs. 7.9 kcal mol^{-1}). The latter represents the rate-limiting step for benzaldehyde, in complete analogy to acetaldehyde. The activity for acetaldehyde is thus computed to be slightly lower than that for benzaldehyde, consistent with the trend of the experimental k_d values (1.14 vs. 1.43 s^{-1}) [99].

Fig. 16 summarizes the structural features of the reaction mechanism for the oxidation of aldehydes by AOR including the adopted protonation states. Different substrates may introduce additional intermediates (as shown for benzaldehyde).

All energies presented up to this point are potential energies (ΔE). However, reaction rates are determined by changes in the free energy (ΔA) of the reacting system. Therefore, the free-energy perturbation (FEP) method was employed to generate free-energy profiles at the DFT(B3LYP)/MM level of theory for the most important reaction steps for the substrate acetaldehyde by sampling along the corresponding reaction paths using molecular dynamics. Furthermore, energy corrections were derived from accurate single-point ab initio calculations using local correlation treatments [LMP2 and LCCSD(T0)] with augmented triple- and quadruple-zeta basis sets. Both types of corrections were combined to determine best estimates of the free energy barriers [21].

While confirming the qualitative mechanistic scenario proposed on the basis of DFT(B3LYP)/MM energy profiles, the ab initio and

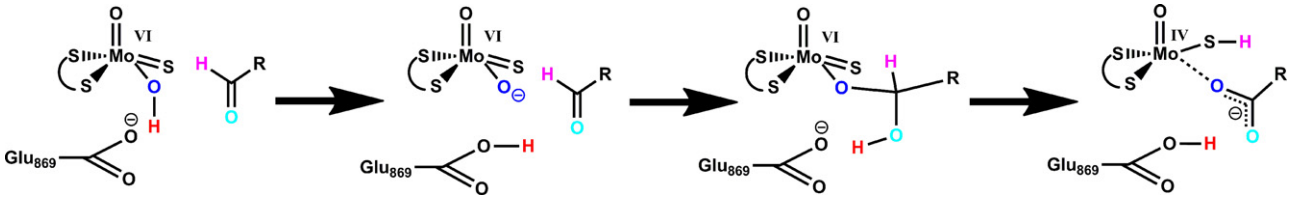

Fig. 16. Generalized scheme of the energetically preferred reaction mechanism of AOR.

FEP QM/MM calculations provide corrections to the barriers that are important when aiming at high accuracy. In the case of AOR, these individual corrections range up to several kcal mol^{-1}, but they tend to compensate each other to some extent in the reactions studied. The best estimates of the free energy barriers differ from the QM(B3LYP/B1)/MM barriers by only about 3 kcal mol^{-1}, and the Lewis base catalyzed mechanism as depicted in Fig. 14 remains preferred over the concerted and the metal center activated pathways [21]. It is thus reassuring that standard DFT/MM applications give qualitative mechanistic insights that withstand scrutiny at higher levels, but it is clearly also desirable to strive for enhanced accuracy both for QM/MM energies and free energies, especially in the case of competing mechanisms with similar barriers.

It has recently been claimed [84] that the cofactor of AOR remains active upon replacing the sulfido by an oxo ligand, in spite of the fact that XO was observed to be deactivated by this modification [83]. Therefore, the oxidation of benzaldehyde was investigated [23] using modified cofactors, with the sulfido ligand substituted by an oxo or a selenido ligand (as found in the related nicotinate dehydrogenase [85]). In both cases, only the final rate-limiting hydride transfer was considered. The computed barrier for the oxo form was prohibitively high (26.6 kcal mol^{-1}), while those for the sulfido and selenido forms were much lower (7.2 and 6.5 kcal mol^{-1}, respectively). These results indicate that the oxo form of the cofactor should indeed be inactive. Some key distances of the optimized stationary points for the hydride transfer step are shown in Fig. 17. It is apparent that the geometrical distortions required to reach the transition state (TS3) are largest for the oxo form, which may explain the exceedingly high barrier.

5.5. QM/MM investigations for xanthine oxidase

XO plays an important role in the catabolism of purines and catalyzes the conversion of hypoxanthine to xanthine and further on to uric acid. In contrast to the situation in AOR, where the substrate orientation is well-defined and only two distinct protonation states need to be taken into account (protonated and deprotonated Glu869), the setup for XO is quite intricate. In total, seven mechanistic variants with different tautomeric forms of xanthine, different protonation states of the active-site residues, and different substrate orientations were considered [20]. Glu802 was taken to be protonated in the enzymatic environment, in agreement with recently published results for XDH [100]. This protonation state is supported by QM/MM calculations in setups with deprotonated Glu802 where geometry optimizations led to spontaneous proton transfer from the substrate to Glu802, which is incompatible with the experimental finding that XO is acting on neutral xanthine [101]. Consistent with the standard protonation state at physiological pH and in agreement with experimental findings [89,101,102], Arg880 was taken to be protonated in all setups. Glu1261 was assumed to act as a Lewis base and was therefore deprotonated, in agreement with the results from the AOR study [19]. Further details on the protonation states of the different setups are given in the original publication [20]. Two different substrate orientations, called "upside" and "upside down", were explored. Since their interconversion is prohibited by the steric constraints in the binding pocket, calculations on large cluster models were performed to establish a common energy scale.

The mechanistic studies started from the product-bound state, which is commonly accepted in the recent literature to be part of the catalytic cycle [89,91,100,102,103]. In the following, only one example of each substrate orientation is presented, namely the most reactive setup with "upside" (Fig. 18) and "upside down" (Fig. 19) orientation. The results for the other five setups (involving other substrate tautomers and other protonation states of the active-site residues) are documented in the literature [20].

For the "upside" orientation, see Fig. 18, the reaction starts with a tautomerization of neutral xanthine from its (N1, N3, N7) form (IUPAC numbering convention), which is predominant in aqueous solution [104], to its (N1, N7, N9) form in IM1′. This is followed by a second proton transfer (via TS1), this time from the molybdenum-attached OH group to Glu1261. The thus activated oxygen at the cofactor then attacks the substrate to form a tetrahedral intermediate (IM2). In the final step, the H8 atom is transferred to the sulfide group of the cofactor. According to the B3LYP/MM relative energies, the overall reaction barrier is determined by the energy difference between the reactant complex and the transition state TS3 for the hydride transfer. It is calculated to be about 20 kcal mol^{-1}, and thus considerably higher than the experimental value of around 15 kcal mol^{-1}. As DFT methods tend to underestimate rather than overestimate energy barriers [105], it is unlikely that this setup represents the enzymatic pathway.

For the "upside down" orientation, see Fig. 19, Glu1261 first deprotonates xanthine at the N3 position (via TS1′), followed by reorientation of the catalytically active OH group via TS1″ and a subsequent proton transfer from the cofactor to the N9 atom of xan-

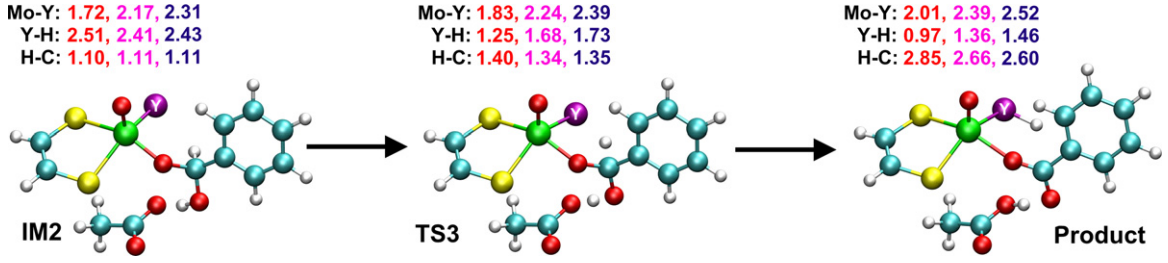

Fig. 17. Hydride transfer reaction for benzaldehyde in AOR [23]. Given are some key distances at the QM(B3LYP/B1)/MM level of theory with Y = O (red), Y = S (pink) and Y = Se (purple).

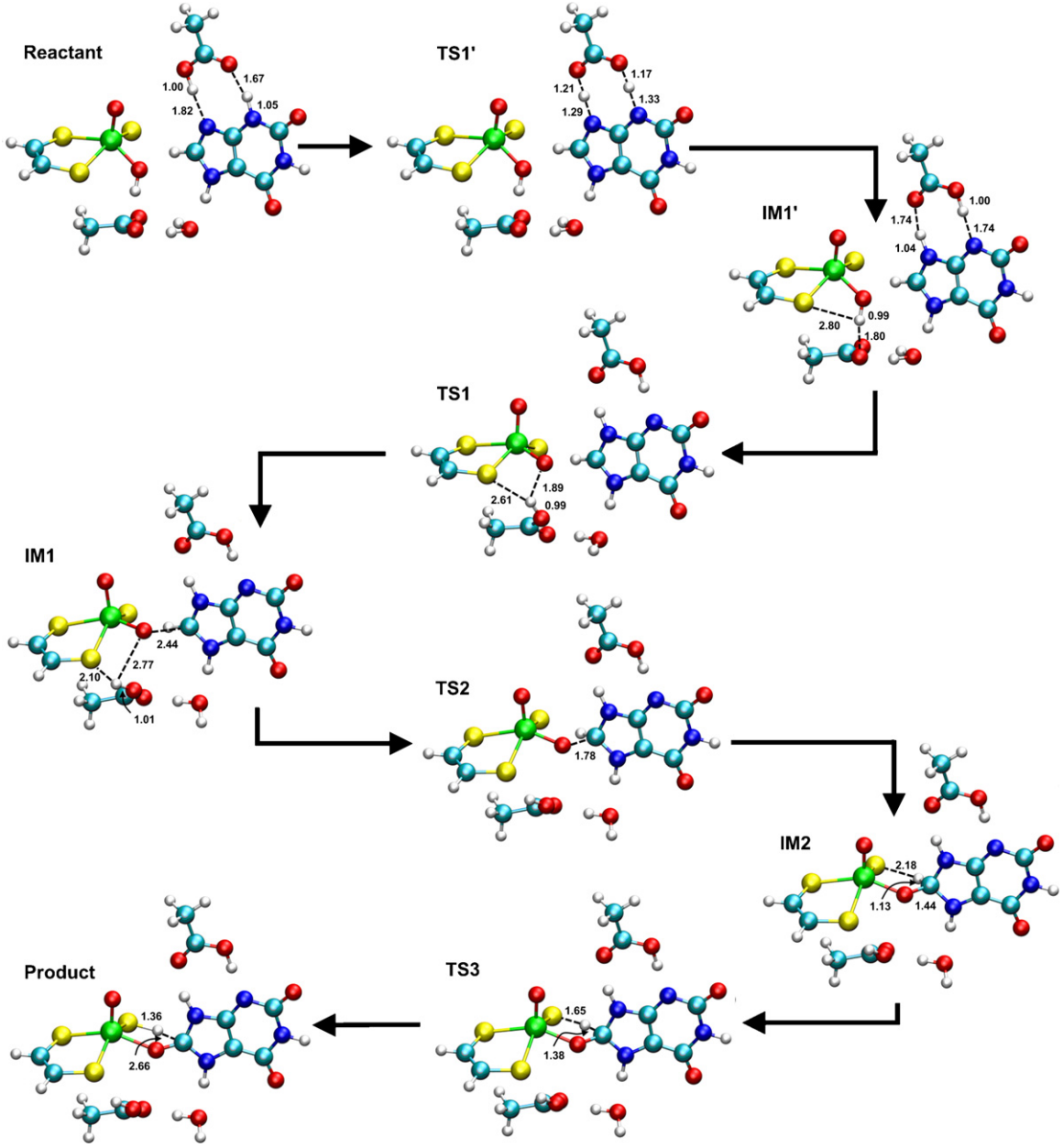

Fig. 18. Reaction mechanism for the oxidation of xanthine by XO with the substrate in "upside" orientation. Reproduced from Ref. [20], with permission of the copyright holders.

thine to form the intermediate IM1. The substrate tautomer and the cofactor are both activated in IM1. They react to form a tetrahedral intermediate (IM2), and a subsequent rate-limiting hydride transfer generates the product. Overall, these latter reaction steps are quite similar for both substrate orientations. However, the pathway with "upside down" orientation is favored, with a barrier of 13–15 kcal mol^{-1} at the B3LYP/MM level that is consistent with the available experimental data [90,106–110].

The barriers presented so far refer to individually prepared setups with QM/MM energies that are not directly comparable among each other. Therefore, cluster calculations [111–114] were performed to establish a common energy scale and to enable comparisons between different setups [20]. These confirm that the "upside" conformation of xanthine leads to the most stable reactant complex, as indicated by a recent X-ray structure [103]. On the other hand, the lowest overall barrier (corresponding to the TS of the hydride transfer, TS3) is obtained for the "upside down" conformation, which should thus be the catalytically active one. This can be attributed to the influence of the Arg880 residue, i.e., the increased electrostatic stabilization of the negatively charged N3 region of the substrate in the tetrahedral intermediate IM2 and the following rate-limiting transition state TS3 [20].

Concerning the role of the active-site residues in the favored mechanism, Glu1261 mediates the conversion of the substrate into its reactive tautomer. This is achieved by deprotonating xanthine at N3 followed by reorientation of the molybdenum-attached OH group and a second proton transfer that activates cofactor and substrate. The Arg880 residue facilitates substrate binding through stabilizing electrostatic interactions, but its main role during the reaction is to stabilize the substrate in the IM2 intermediate and the preceding (TS2) and following (TS3) transition states, especially by the interaction with the negatively charged N3 atom. The Glu802 residue seems to have a relatively minor

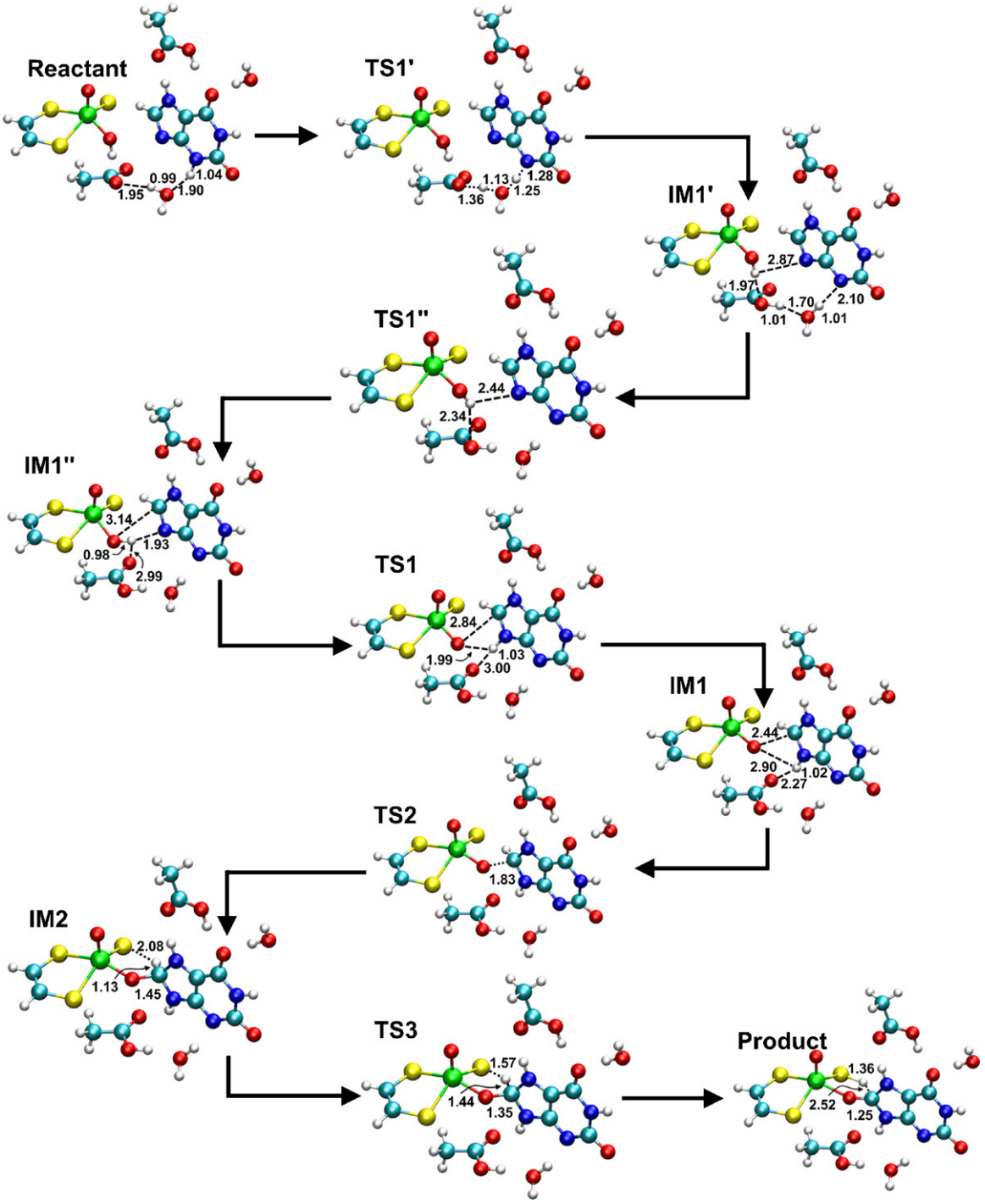

Fig. 19. Reaction mechanism for the oxidation of xanthine by XO with the substrate in "upside down" orientation. Reproduced from Ref. [20], with permission of the copyright holders.

effect on the catalytic activity in XO which is reduced but not lost upon Glu802 → Gln802 mutation in xanthine dehydrogenase (XDH) [100]. A separate QM/MM study of the corresponding XO mutant [22] showed that xanthine still reacts in the "upside down" orientation, but the hydrogen bonding pattern around Gln802 is different so that a slightly different pathway becomes favored. Compared with the wild-type enzyme, this leads to a somewhat higher barrier (by 2–3 kcal mol^{-1}) [22], similar to the experimental findings for XDH [100].

According to the QM/MM calculations, the most favorable pathways in AOR [19] and XO [20] involve Lewis base catalysis by an active-site Glu residue. They share a number of characteristic features, especially in the later stages of the reaction, see Figs. 16 and 20. In AOR acting on acetaldehyde as substrate, there are alternative one-step and metal center activated mechanisms [19] which are not feasible in AOR with larger substrates such as benzaldehyde and in XO, because of the much more specific substrate binding [20]. The QM/MM results are broadly compatible with previous mechanistic notions about the reductive half-reaction in AOR and XO, but go significantly beyond them by offering insights that are hard to unravel by other means, e.g., with regard to substrate orientation, the determination of

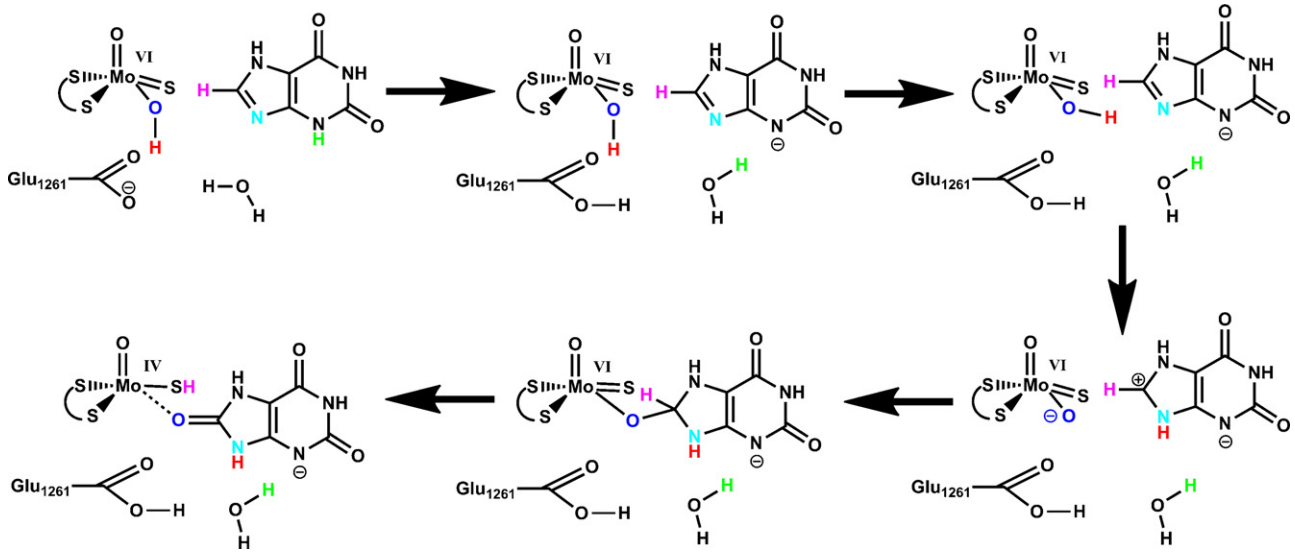

Fig. 20. Scheme of the preferred reaction mechanism of XO acting on xanthine as substrate.

the catalytically active species, and the role of individual residues in XO.

The different reactivity of two xanthine-related substrates provides experimental evidence [110,115] that supports the "upside down" orientation predicted by the QM/MM calculations (see Fig. 21). In the "upside" orientation, both substrates would interact with Arg880 in exactly the same manner via O6 (structures A and B), and they should therefore exhibit similar reactivity (contrary to experiment). In the "upside-down" orientation, the inactive substrate 1-methyl-6-oxopurine (structure C) is stabilized in its reactive form by Arg880 much less than the active substrate 1-methyl-2,6-dioxopurine (structure D).

Further insight into the role of the active-site environment can be gained by comparing the QM/MM results for the enzymatic reaction with DFT results for a gas-phase model reaction. In the case of the oxidation of xanthine by XO, this was done [20] by re-optimizing the stationary points of the most favorable pathway for a minimal model system (part of the cofactor plus substrate, starting from the optimized QM/MM structures and using the same DFT approach as in the QM/MM calculation). It was found that the reaction mechanism (from IM1″ onwards, see Fig. 19) remains qualitatively the same. In the initial stage of the reaction, the relative orientations of cofactor and substrate change upon gas-phase re-optimization (due to the missing constraints from the protein environment) which leads to a lowering of the energy profile. By contrast, in the latter stage, the geometries do not change much, and the energy profile is raised because of the missing electrostatic stabilization of IM2 and TS3 by Arg880 (see Fig. 19). As a consequence, the overall barrier is increased by about 4 kcal mol^{-1} (DFT model vs. QM/MM) which translates into a decrease of the rate by a factor of about 10^3. In addition, it should be emphasized that the most favorable pathway in the enzyme involves a xanthine tautomer which is rather unstable in the gas phase and is strongly stabilized in the enzyme by electrostatic interactions with Arg880. In this situation, gas-phase model studies run the risk of assuming the wrong tautomer to be reactive; this is avoided in the comparisons described above by starting from QM/MM optimized geometries containing the right tautomer.

To assess the reactivity of a substrate other than xanthine [22], the oxidation of 2-oxo-6-methylpurine by XO was investigated. The calculated pathways for three possible tautomers were similar to those found previously for xanthine, contrary to claims in the literature [89,102] that these two substrates follow substan-

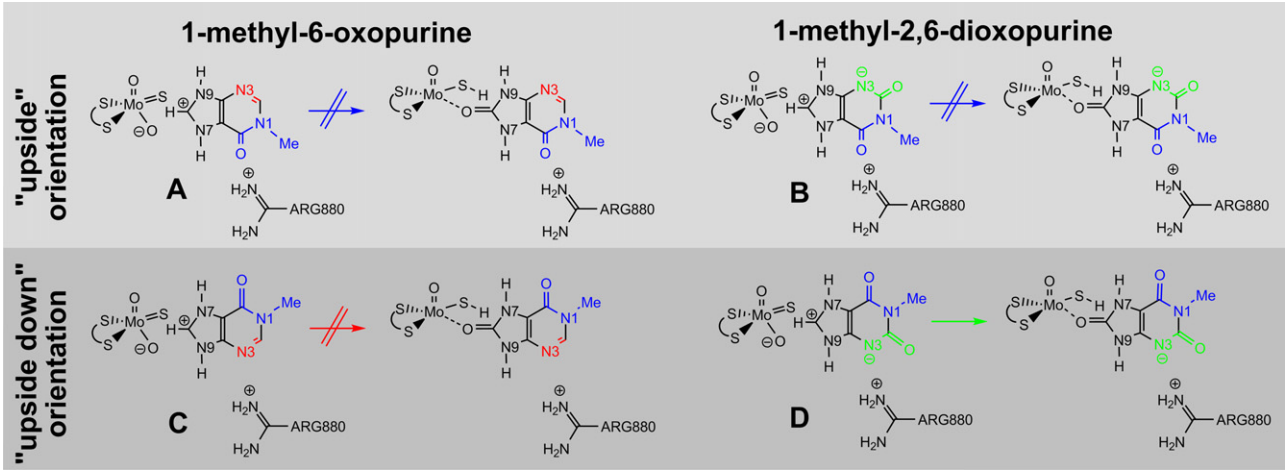

Fig. 21. Reactivity control by the substrate-Arg880 interaction rationalizes the different reactivity of 1-methyl-6-oxopurine and 1-methyl-2,6-dioxopurine, see text. Reproduced from Ref. [20], with permission of the copyright holders.

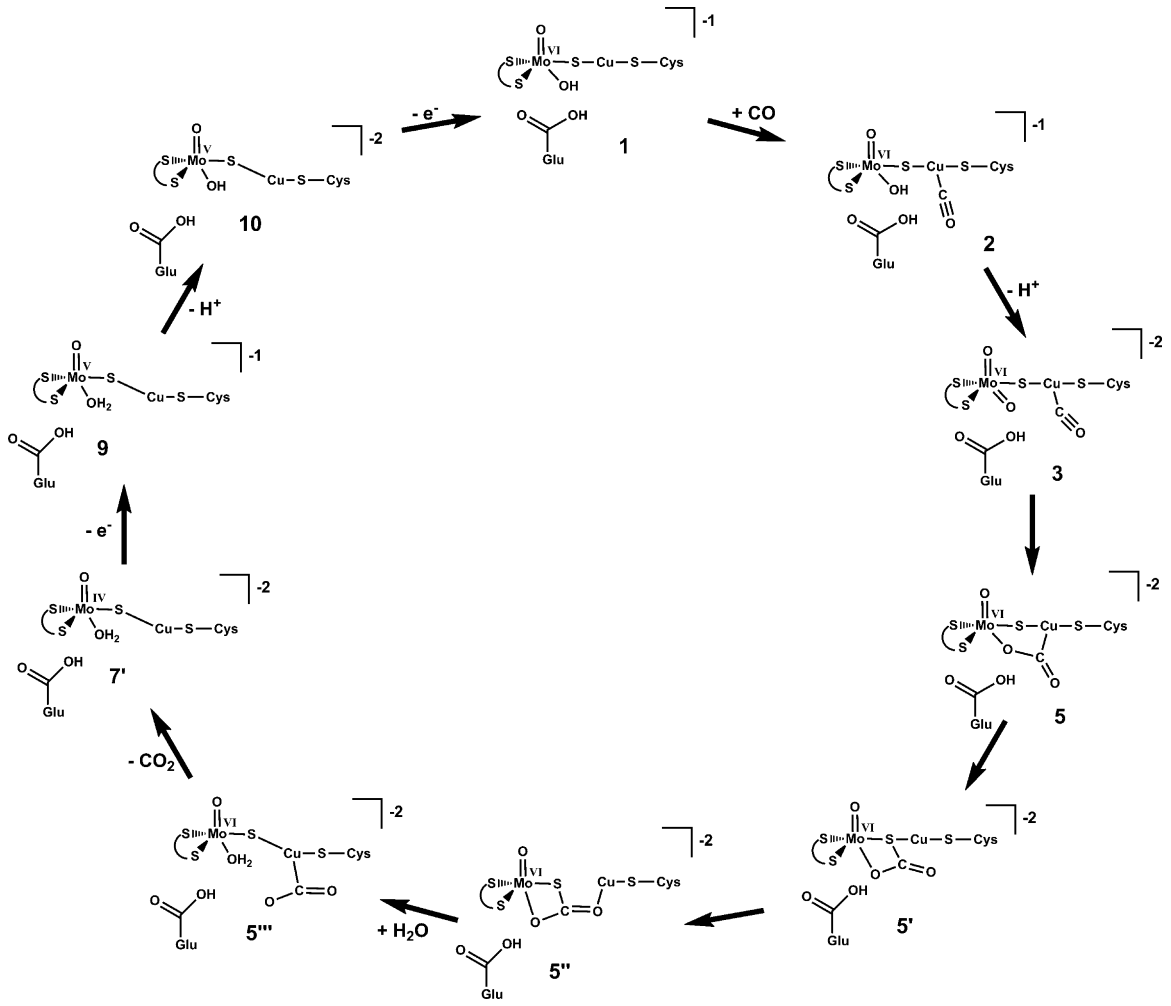

Fig. 22. Reaction mechanism of CO dehydrogenase as reported by Siegbahn and Shestakov [118]. The numbering and the assigned oxidation states follow the original publication.

tially different reaction paths. According to the B3LYP/MM results for the largest QM region, rate-limiting barriers of 25.8, 7.3, and 11.3 kcal mol^{-1} were obtained for the three tautomers. The highest value corresponds to the setup with the most stable gas-phase tautomer. Therefore, as in the case of xanthine, the kinetically active setups involve tautomers other than the lowest-energy gas-phase species. The overall barriers for these two setups are of comparable size, but somewhat lower than the value of 14.8 kcal mol^{-1} derived from experiment [116]. However, the QM/MM calculations show the right trend in predicting 2-oxo-6-methylpurine to be oxidized faster by XO than xanthine. This finding is supported by QM model studies for the two substrates, which show the higher reactivity of 2-oxo-6-methylpurine to be an intrinsic feature of the substrate [22].

As in the case of AOR, further QM(B3LYP/B1)/MM calculations were performed for XO to check the effects of replacing the sulfido ligand in the cofactor by an oxo or a selenido ligand. The complete reaction paths for the oxidation of xanthine by XO were re-optimized for the oxo and selenido forms to determine the changes in the barriers for each individual step [22]. Only the final hydride transfer step was significantly influenced by the modification of the cofactor. The oxo form was found to be inactive, with a barrier of 20.3 kcal mol^{-1} for hydride transfer and an overall barrier of 30.6 kcal mol^{-1}. The corresponding values for the sulfido form were 7.0 and 13.1 kcal mol^{-1}, while those for the selenido form were 4.9 and 10.9 kcal mol^{-1}, respectively. These results are consistent with the experimentally observed lack of activity of the oxo form of XO [83] and with a slightly increased reactivity of the selenido form, as previously suggested on the basis of experimental and theoretical evidence [85]. Overall, AOR and XO thus behave analogously upon modification of the cofactor [22]. In both cases, the barrier for the final hydride transfer step becomes very high in the oxo form which can be traced back to the geometrical requirements for this rearrangement [22]. Given these similarities, it seems unlikely that the cofactor of AOR may contain an oxo rather than a sulfido group in its active form.

6. Further enzymes

6.1. CO dehydrogenase

Another molybdopterin-containing enzyme that does not belong to one of the above families is CO dehydrogenase. It catalyzes the oxidation of CO to CO_2. Based on an updated crystal structure [117] which showed the presence of a copper atom in the vicinity of the molybdenum center (see Fig. 22), Siegbahn and Shestakov performed a B3LYP study of the catalytic mechanism using relatively large chemical models with several (partially constrained) side chains of active-site residues included [118]. The original calculations identified a pathway with a low barrier for C–O bond formation and CO_2 release, with an overall barrier of 21.0 kcal mol^{-1}. However, experiments with an *n*-butylisocyanide

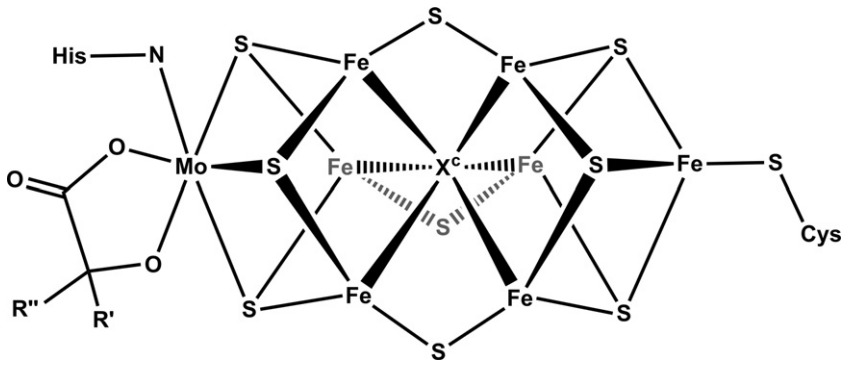

Fig. 23. The FeMo cofactor, including the interstitial atom X^c, the homocitrate ligand (left), and two residues linking the cofactor to the apo enzyme, His (left) and Cys (right).

inhibitor [117,119] indicated the formation of an intermediate S–CO_2 species that had not been considered in this mechanism. When the mechanistic search was extended to include SCO_2 structures, they were deep minima, making CO_2 release much more difficult than in the originally proposed pathway. Hence, further calculations were performed, covering other spin states, a varying number of protons and electrons, and additional water molecules. This led to a plausible pathway for S–C bond cleavage, with an overall barrier of 18.9 kcal mol^{-1}, in which a water molecule is inserted between the molybdenum center and the SCO_2 group. The intermediates of this catalytic cycle are depicted in Fig. 22.

6.2. Nitrogenase

Nitrogenases reduce nitrogen (N_2) to ammonia (NH_3). The most common Mo-containing form of nitrogenase consists of two metalloproteins, the Fe- and the MoFe-protein. In the latter, a molybdenum atom is incorporated in a $MoFe_7S_9X$ cluster, as shown in Fig. 23. There have been numerous theoretical investigations on these enzymes, especially on the nature of the interstitial atom X^c in the cofactor and on the reaction mechanism. A thorough review of these studies is beyond the scope of this article. Early results have been summarized in this journal [120], covering work from a period when the interstitial atom had not yet been discov-

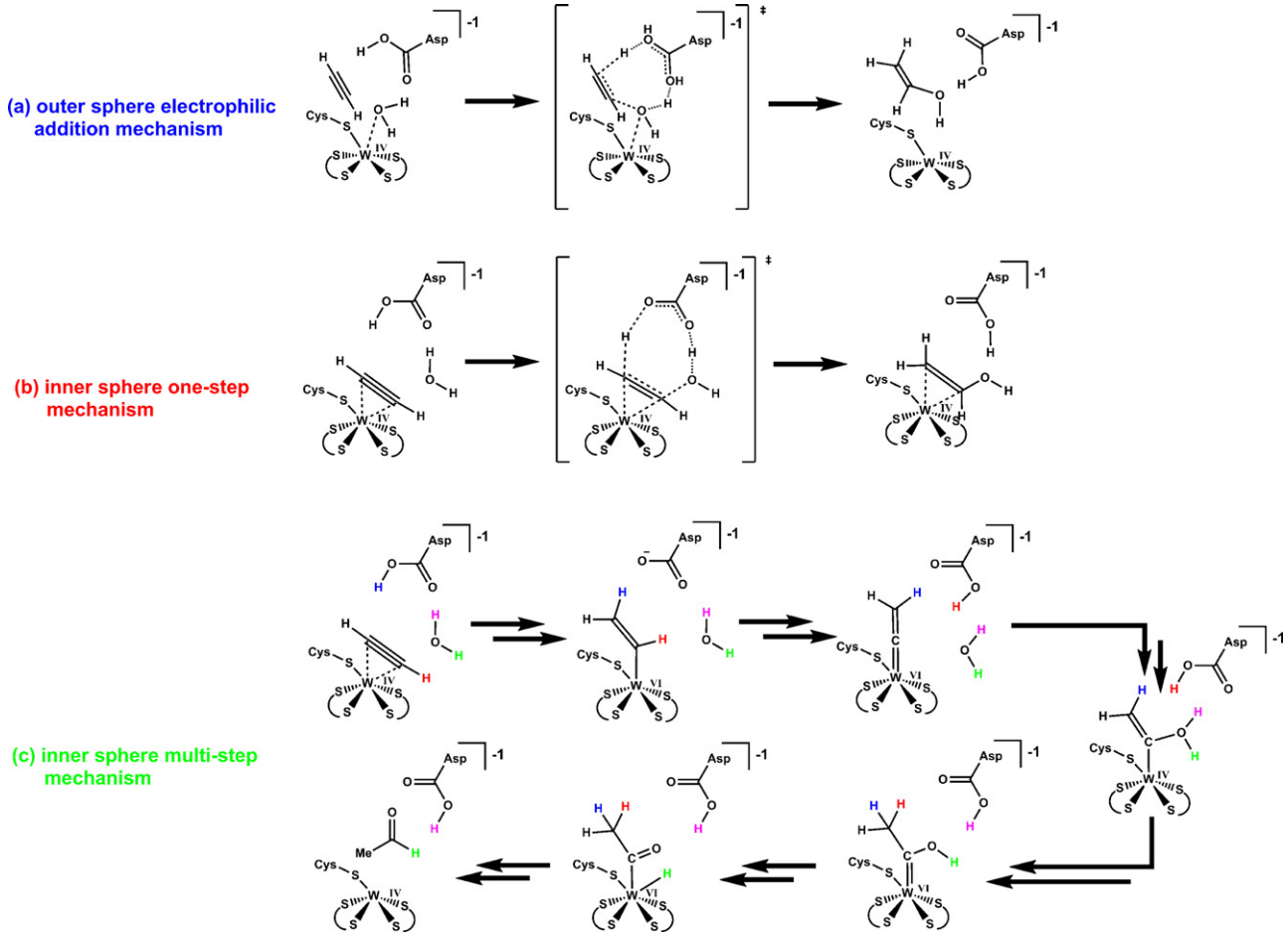

Fig. 24. Investigated reaction mechanisms for models of acetylene hydratase. Transition states are depicted for the one-step mechanisms (a) and (b), while only the key intermediates (numbered as in the original publication) are given for (c). The original publication [144] provides all transition states and some additional intermediates (involving conformational changes).

ered [121]. For later contributions on the nature of the interstitial atom, we refer the reader to the original publications employing QM gas-phase models [122–125] and QM/MM techniques [18]. According to these studies, X^c is most likely a nitrogen atom, and this assumption is made in most of the ensuing mechanistic studies. For the latter work, we again refer the reader to the original literature, especially to the QM model studies of Hinnemann and Nørskov [126,127], Kästner and Blöchl [128–131], McKee [132,133], and Dance [134–141]. These QM calculations differ in the assumed reduction state of the cofactor, its protonation state, and the sequence of protonation and nitrogenation. The probably most detailed mechanism has been proposed by Dance [139], involving as many as 21 elementary steps.

6.3. Tungsten-containing enzymes

There are only few computational investigations on tungsten-containing enzymes or models thereof. In the earliest publications on this topic, tungsten was inserted into corresponding optimized molybdenum active sites (replacing molybdenum), to model the difference between the two metals [35,47]. The only mechanistic studies on a tungsten-containing enzyme address acetylene hydratase (AH). DFT calculations on gas-phase models derived from the recently published crystal structure [142] indicated that the exchange of a tungsten-coordinated water molecule against acetylene should be facile [143], and it was therefore concluded that catalysis by AH should proceed via a tungsten–acetylene complex, rather than by the attack of a tungsten-bound water molecule on a solvated acetylene as originally suggested [142]. The former mechanism may rationalize why tungsten is better suited than molybdenum for AH catalysis: the tungsten 5d orbitals are larger than the molybdenum 4d orbitals and should thus interact more strongly with the π-MOs of the acetylene [143]. It should be pointed out, however, that transition states were not located in this work [143], and hence there are no computed barriers that would distinguish between different possible mechanisms. Such comparisons were performed in a later DFT study [144] which addressed three mechanisms, see Fig. 24: (a) an outer-sphere electrophilic addition, (b) an inner-sphere one-step reaction of side-bound acetylene with a free water molecule as proposed earlier [143], and (c) an inner-sphere multi-step pathway involving vinylidene and carbene intermediates. The latter mechanism was found [144] to be kinetically favored by a large margin, with a computed overall barrier of 29 kcal mol^{-1} for (c) compared with 41–44 kcal mol^{-1} for (a) and (b).

7. Conclusions

Theoretical investigations are now available for all three molybdopterin-containing enzyme families as well as for some other molybdenum- and tungsten-containing enzymes. They comprise pure DFT studies on simplified gas-phase model systems and QM/MM studies on whole solvated enzymes. DFT model studies may provide useful insight into intrinsic reactivities and help to distinguish between different possible reaction mechanisms, especially when the computed rate-limiting barriers differ by a large margin. They may also give valuable information on the electronic structure of the transition states and intermediates along various reaction pathways. Most of the DFT studies reviewed here employ model systems consisting of (part of) the cofactor and the substrate, and thus do not capture the influence of the protein environment. This can be included at the DFT level by using successively larger model systems or (more naturally) by QM/MM calculations on the complete enzyme. The available QM/MM studies on AOR and XO indeed show the crucial role of several active-site residues with regard to enzymatic reactivity.

The QM/MM calculations on XO may serve as an example for the insights that can be obtained. They led to a multi-step Lewis base catalyzed mechanism that involves the activation of the cofactor by proton transfer to an active-site residue and the transformation of the substrate from the most stable into the most reactive tautomer, in order to facilitate the subsequent product-forming steps. These calculations clarified the essential role of the active-site environment (Glu802, Glu1261, Arg880) and identified the kinetically preferred orientation of the substrate. Further QM/MM studies explored reactivity changes upon modification of the cofactor, mutation of the Glu802 residue, and use of a different substrate, with results that were compatible with the published experimental data. Combining the available theoretical and experimental evidence we thus end up with a comprehensive and detailed mechanistic picture of biocatalysis by XO.

Generally speaking, theoretical calculations have now advanced to a point where they are able to unravel enzymatic reaction mechanisms and to provide detailed information on the energies, structures, electron densities, spin densities, and spectroscopic properties of all relevant reactive species. They can thus serve as an analytic tool in enzymology that is complementary to experimental analysis.

Note added in proof

Two crystal structures of the urate bound form of xanthine oxidoreductase were reported [145] that confirm the substrate orientation found in the QM/MM work [20]. On the basis of DFT calculations for a large cluster model, a new mechanism was proposed for the reaction catalyzed by the tungsten-dependent acetylene hydratase [146]. These two papers appeared after submission of this article.

Acknowledgment

This work was supported by the Max-Planck-Society.

References

[1] W. Koch, M.C. Holthausen, A Chemist's Guide to Density Functional Theory, 2nd ed., Wiley-VCH, Weinheim, 2001.
[2] E.R. Davidson, Chem. Rev. 100 (2000) 351.
[3] P. Hohenberg, W. Kohn, Phys. Rev. B 136 (1964) 854.
[4] W. Kohn, L.J. Sham, Phys. Rev. A 140 (1965) 1133.
[5] M.R.A. Blomberg, P.E.M. Siegbahn, S. Styring, G.T. Babcock, B. Åkermark, P. Korall, J. Am. Chem. Soc. 119 (1997) 8285.
[6] P.E.M. Siegbahn, M.R.A. Blomberg, Annu. Rev. Phys. Chem. 50 (1999) 221.
[7] P.E.M. Siegbahn, M.R.A. Blomberg, Chem. Rev. 100 (2000) 421.
[8] F. Ogliaro, N. Harris, S. Cohen, M. Filatov, S.P. de Visser, S. Shaik, J. Am. Chem. Soc. 122 (2000) 8977.
[9] S.P. de Visser, F. Ogliaro, N. Harris, S. Shaik, J. Am. Chem. Soc. 123 (2001) 3037.
[10] J.C. Schöneboom, H. Lin, N. Reuter, W. Thiel, S. Cohen, F. Ogliaro, S. Shaik, J. Am. Chem. Soc. 124 (2002) 8142.
[11] A. Ghosh, P.R. Taylor, Curr. Opin. Chem. Biol. 7 (2003) 113.
[12] P.E.M. Siegbahn, M.R.A. Blomberg, Phil. Trans. R. Soc. Lond. A 363 (2005) 847.
[13] A. Warshel, M. Levitt, J. Mol. Biol. 103 (1976) 227.
[14] H.M. Senn, W. Thiel, Top. Curr. Chem. 268 (2007) 173.
[15] H.M. Senn, W. Thiel, Angew. Chem., Int. Ed. 48 (2009) 1198.
[16] M. Leopoldini, N. Russo, M. Toscano, M. Dulak, T.A. Wesolowski, Chem. Eur. J. 12 (2006) 2532.
[17] M. Mohr, J.P. McNamara, H. Wang, S.A. Rajeev, J. Ge, C.A. Morgado, I.H. Hillier, Faraday Discuss. 124 (2003) 413.
[18] H. Xie, R. Wu, Z. Zhou, Z. Cao, J. Phys. Chem. B 112 (2008) 11435.
[19] S. Metz, D. Wang, W. Thiel, J. Am. Chem. Soc. 131 (2009) 4628.
[20] S. Metz, W. Thiel, J. Am. Chem. Soc. 131 (2009) 14885.
[21] J.M. Dieterich, H.J. Werner, R.A. Mata, S. Metz, W. Thiel, J. Chem. Phys. 132 (2010) 035101.
[22] S. Metz, W. Thiel, J. Phys. Chem. B 114 (2010) 1506.
[23] S. Metz, QM/MM Investigations on the Hydroxylation Reactions of Molybdopterin-containing Enzymes, Ph.D. Thesis, Heinrich-Heine-Universität Düsseldorf, 2009.
[24] U.C. Singh, P.A. Kollman, J. Comput. Chem. 7 (1986) 718.
[25] M. Svensson, S. Humbel, R.D.J. Froese, T. Matsubara, S. Sieber, K. Morokuma, J. Phys. Chem. 100 (1996) 19357.

[26] S. Humbel, S. Sieber, K. Morokuma, J. Chem. Phys. 105 (1996) 1959.
[27] S. Dapprich, I. Komáromi, K.S. Byun, K. Morokuma, M.J. Frisch, J. Mol. Struct. (Theochem) (1999) 461.
[28] T. Vreven, K. Morokuma, J. Comput. Chem. 21 (2000) 1419.
[29] T. Vreven, B. Mennucci, C.O. da Silva, K. Morokuma, J. Tomasi, J. Chem. Phys. 115 (2001) 62.
[30] T. Vreven, K. Morokuma, Ö. Farkas, M.J. Frisch, J. Comput. Chem. 24 (2003) 760.
[31] A.H. de Vries, P. Sherwood, S.J. Collins, A.M. Rigby, M. Rigutto, G.J. Kramer, J. Phys. Chem. B 103 (1999) 6133.
[32] P. Sherwood, A.H. de Vries, S.J. Collins, S.P. Greatbanks, N.A. Burton, M.A. Vincent, I.H. Hillier, Faraday Discuss. (1997) 79.
[33] C.V. Sumowski, C. Ochsenfeld, J. Phys. Chem. A 113 (2009) 11734.
[34] M. Leopoldini, T.M. Marino, d.C. Michelini, I. Rivalta, N. Russo, E. Sicilia, M. Toscano, Theor. Chem. Acc. 117 (2007) 765.
[35] M. Hofmann, J. Biol. Inorg. Chem. 12 (2007) 989.
[36] A. Thapper, R.J. Deeth, E. Nordlander, Inorg. Chem. 38 (1999) 1015.
[37] M. Hoffman, J. Biol. Inorg. Chem. 14 (2009) 1023.
[38] N.M.F.S.A. Cerqueira, P.J. Gonzalez, C.D. Brondino, M.J. Romão, C.C. Romão, I. Moura, J.J.G. Moura, J. Comput. Chem. 30 (2009) 2466.
[39] H. Xie, Z. Cao, Organometallics 29 (2009) 436.
[40] C.E. Webster, M.B. Hall, J. Am. Chem. Soc. 123 (2001) 5820.
[41] B.L. Vallee, R.J.P. Williams, Proc. Natl. Acad. Sci. U.S.A. 59 (1968) 498.
[42] R.J.P. Williams, Eur. J. Biochem. 234 (1995) 363.
[43] B.S. Lim, J.P. Donahue, R.H. Holm, Inorg. Chem. 39 (2000) 263.
[44] J.P. Ridge, K.-F. Aguey-Zinsou, P.V. Bernhardt, I.M. Brereton, G.R. Hanson, A.G. McEwan, Biochemistry 41 (2002) 15762.
[45] N. Cobb, C. Hemann, G.A. Polsinelli, J.P. Ridge, A.G. McEwan, R. Hille, J. Biol. Chem. 282 (2007) 35519.
[46] A. Thapper, R.J. Deeth, E. Nordlander, Inorg. Chem. 41 (2002) 6695.
[47] J.P. McNamara, I.H. Hillier, T.S. Bhachu, C.D. Garner, Dalton Trans. (2005) 3572.
[48] J.P. McNamara, J.A. Joule, I.H. Hillier, C.D. Garner, Chem. Commun. (2005) 177.
[49] M. Kaupp, Angew. Chem., Int. Ed. 43 (2004) 546.
[50] E. Hernandez-Marin, T. Ziegler, Can. J. Chem. 88 (2010) 683.
[51] M. Hofmann, J. Mol. Struct. (Theochem) 773 (2006) 59.
[52] M. Hofmann, Inorg. Chem. 47 (2008) 5546.
[53] M. Szaleniec, C. Hagel, M. Menke, P. Nowak, M. Witko, J. Heider, Biochemistry 46 (2007) 7637.
[54] M. Szaleniec, M. Witko, J. Heider, J. Mol. Catal. A: Chem. 286 (2008) 128.
[55] D.P. Kloer, C. Hagel, J. Heider, G.E. Schulz, Structure 14 (2006) 1377.
[56] M. Szaleniec, T. Borowski, K. Schühle, M. Witko, J. Heider, J. Am. Chem. Soc. 132 (2010) 6014.
[57] K. Pal, P.K. Chaudhury, S. Sarkar, Chem. Asian J. 2 (2007) 956.
[58] H.L. Wilson, K.V. Rajagopalan, J. Biol. Chem. 279 (2004) 15105.
[59] E. Hernandez-Marin, T. Ziegler, Inorg. Chem. 48 (2009) 1323.
[60] M.J. Romão, N. Rösch, R. Huber, J. Biol. Inorg. Chem. 2 (1997) 782.
[61] R.R. Mendel, G. Schwarz, Crit. Rev. Plant Sci. 18 (1999) 33.
[62] M.R. Bray, R.J. Deeth, Inorg. Chem. 35 (1996) 5720.
[63] M.R. Bray, R.J. Deeth, J. Chem. Soc., Dalton Trans. (1997) 1267.
[64] A.A. Voityuk, K. Albert, S. Kostlmeier, V.A. Nasluzov, K.M. Neyman, P. Hof, R. Huber, M.J. Romão, N. Rösch, J. Am. Chem. Soc. 119 (1997) 3159.
[65] T.D. Tullius, D.M. Kurtz, K.O. Hodgson, J. Am. Chem. Soc. 101 (1979) 2776.
[66] J. Bordas, R.C. Bray, C.D. Garner, S. Gutteridge, S. Hasnain, Biochem. J. 191 (1980) 499.
[67] S.P. Cramer, R. Wahl, K.V. Rajagopalan, J. Am. Chem. Soc. 103 (1981) 7721.
[68] S.P. Cramer, R. Hille, J. Am. Chem. Soc. 107 (1985) 8164.
[69] R. Hille, G.N. George, M.K. Eidsness, S.P. Cramer, Inorg. Chem. 28 (1989) 4018.
[70] N.A. Turner, R.C. Bray, G.P. Diakun, Biochem. J. 260 (1989) 563.
[71] C.J. Doonan, A. Stockert, R. Hille, G.N. George, J. Am. Chem. Soc. 127 (2005) 4518.
[72] R. Hille, Chem. Rev. 96 (1996) 2757.
[73] C. Kisker, H. Schindelin, D.C. Rees, Annu. Rev. Biochem. 66 (1997) 233.
[74] G. Schwarz, R.R. Mendel, Annu. Rev. Plant Biol. 57 (2006) 623.
[75] P. Ilich, R. Hille, Inorg. Chim. Acta 263 (1997) 87.
[76] A.A. Voityuk, K. Albert, M.J. Romão, R. Huber, N. Rösch, Inorg. Chem. 37 (1998) 176.
[77] P. Ilich, R. Hille, J. Phys. Chem. B 103 (1999) 5406.
[78] X.H. Zhang, Y.D. Wu, Inorg. Chem. 44 (2005) 1466.
[79] T. Amano, N. Ochi, H. Sato, S. Sakaki, J. Am. Chem. Soc. 129 (2007) 8131.
[80] J.F. Alfaro, J.P. Jones, J. Org. Chem. 73 (2008) 9469.
[81] C.A. Bayse, Dalton Trans. (2009) 2306.
[82] R. Huber, P. Hof, R.O. Duarte, J.J.G. Moura, I. Moura, M.Y. Liu, J. LeGall, R. Hille, M. Archer, M.J. Romão, Proc. Natl. Acad. Sci. U.S.A. 93 (1996) 8846.
[83] V. Massey, D. Edmondson, J. Biol. Chem. 245 (1970) 6595.
[84] T. Santos-Silva, F. Ferroni, A. Thapper, J. Marangon, P.J. González, A. Rizzi, I. Moura, J.J.G. Moura, M.J. Romão, C.D. Brondido, J. Am. Chem. Soc. 131 (2009) 7990.
[85] N. Wagener, A.J. Pierek, A. Ibdah, R. Hille, H. Dobbek, Proc. Natl. Acad. Sci. U.S.A. 106 (2009) 11055.
[86] B.D. Howes, R.C. Bray, R.L. Richards, N.A. Turner, B. Bennett, D.J. Lowe, Biochemistry 35 (1996) 1432.
[87] P. Manikandan, E.Y. Choi, R. Hille, B.M. Hoffman, J. Am. Chem. Soc. 123 (2001) 2658.
[88] R. Hille, Arch. Biochem. Biophys. 433 (2005) 107.
[89] J.M. Pauff, C.F. Hemann, N. Jünemann, S. Leimkühler, R. Hille, J. Biol. Chem. 282 (2007) 12785.
[90] Y. Yamaguchi, T. Matsumura, K. Ichida, K. Okamoto, T. Nishino, J. Biochem. 141 (2007) 513.
[91] T. Nishino, K. Okamoto, B.T. Eger, E.F. Pai, T. Nishino, FEBS J. 275 (2008) 3278.
[92] R. Hille, H. Sprecher, J. Biol. Chem. 262 (1987) 10914.
[93] P.C. Hariharan, J.A. Pople, Theor. Chim. Acta 28 (1973) 213.
[94] T. Clark, J. Chandrasekhar, G.W. Spitznagel, P.v.R. Schleyer, J. Comput. Chem. 4 (1983) 294.
[95] W.R. Wadt, P.J. Hay, J. Chem. Phys. 82 (1985) 284.
[96] A. Höllwarth, M. Böhme, S. Dapprich, A.W. Ehlers, A. Gobbi, V. Jonas, K.F. Köhler, R. Stegmann, A. Veldkamp, G. Frenking, Chem. Phys. Lett. 208 (1993) 237.
[97] P.J. Hay, W.R. Wadt, J. Chem. Phys. 82 (1985) 270.
[98] A.W. Ehlers, M. Böhme, S. Dapprich, A. Gobbi, A. Höllwarth, V. Jonas, K.F. Köhler, R. Stegmann, A. Veldkamp, G. Frenking, Chem. Phys. Lett. 208 (1993) 111.
[99] B.A.S. Barata, J. LeGall, J.J.G. Moura, Biochemistry 32 (1993) 11559.
[100] U. Dietzel, J. Kuper, J.A. Doebbler, A. Schulten, J.J. Truglio, S. Leimkühler, C. Kisker, J. Biol. Chem. 284 (2009) 8768.
[101] J.H. Kim, M.G. Ryan, H. Knaut, R. Hille, J. Biol. Chem. 271 (1996) 6771.
[102] J.M. Pauff, J.J. Zhang, C.E. Bell, R. Hille, J. Biol. Chem. 283 (2008) 4818.
[103] J.M. Pauff, H. Cao, R. Hille, J. Biol. Chem. 284 (2009) 8760.
[104] E. Kulikowska, B. Kierdaszuk, D. Shugar, Acta Biochim. Pol. 51 (2004) 493.
[105] A.J. Cohen, P. Mori-Sánchez, W. Yang, Science 321 (2008) 792.
[106] D. Edmondson, D. Ballou, A. Vanheuve, G. Palmer, V. Massey, J. Biol. Chem. 248 (1973) 6135.
[107] J.S. Olson, D.P. Ballou, G. Palmer, V. Massey, J. Biol. Chem. 249 (1974) 4350.
[108] M.S. Mondal, S. Mitra, Biochemistry 33 (1994) 10305.
[109] A.L. Stockert, S.S. Shinde, R.F. Anderson, R. Hille, J. Am. Chem. Soc. 124 (2002) 14554.
[110] E.Y. Choi, A.L. Stockert, S. Leimkühler, R. Hille, J. Inorg. Biochem. 98 (2004) 841.
[111] R. Sevastik, F. Himo, Bioorg. Chem. 35 (2007) 444.
[112] K.H. Hopmann, F. Himo, J. Chem. Theory Comput. 4 (2008) 1129.
[113] S.-L. Chen, W.-H. Fang, F. Himo, Theor. Chem. Acc. 120 (2008) 515.
[114] P.E.M. Siegbahn, F. Himo, J. Biol. Inorg. Chem. 14 (2009) 643.
[115] F. Bergmann, H. Kwietny, G. Levin, D.J. Brown, J. Am. Chem. Soc. 82 (1960) 598.
[116] R.B. McWhirter, R. Hille, J. Biol. Chem. 266 (1991) 23724.
[117] H. Dobbek, L. Gremer, R. Kiefersauer, R. Huber, O. Meyer, Proc. Natl. Acad. Sci. U.S.A. 99 (2002) 15971.
[118] P.E.M. Siegbahn, A.F. Shestakov, J. Comput. Chem. 26 (2005) 888.
[119] H. Dobbek, L. Gremer, O. Meyer, R. Huber, in: I. Bertini, H. Sigel (Eds.), Handbook on Metalloproteins, Marcel Dekker, New York, 2001, p. 1136.
[120] F. Barrière, Coord. Chem. Rev. 236 (2003) 71.
[121] O. Einsle, F.A. Tezcan, S.L.A. Andrade, B. Schmidt, M. Yoshida, J.B. Howard, D.C. Rees, Science 297 (2002) 1696.
[122] B. Hinnemann, J.K. Nørskov, J. Am. Chem. Soc. 125 (2003) 1466.
[123] T. Lovell, T.Q. Liu, D.A. Case, L. Noodleman, J. Am. Soc. Chem. 125 (2003) 8377.
[124] I. Dance, Chem. Commun. 3 (2003) 324.
[125] U. Huniar, R. Ahlrichs, D. Coucouvanis, J. Am. Chem. Soc. 126 (2004) 2588.
[126] B. Hinnemann, J.K. Nørskov, J. Am. Chem. Soc. 126 (2004) 3920.
[127] B. Hinnemann, J.K. Nørskov, Top. Catal. 37 (2006) 55.
[128] J. Schimpl, H.M. Petrilli, P.E. Blöchl, J. Am. Chem. Soc. 125 (2003) 15772.
[129] J. Kästner, P.E. Blöchl, J. Chem. Phys. 123 (2005) 074306.
[130] J. Kästner, P.E. Blöchl, ChemPhysChem 6 (2005) 1724.
[131] J. Kästner, P.E. Blöchl, J. Am. Chem. Soc. 129 (2007) 2998.
[132] M.L. McKee, J. Comput. Chem. 28 (2007) 1342.
[133] M.L. McKee, J. Comput. Chem. 28 (2007) 1796.
[134] L.C. Seefeldt, I. Dance, D.R. Dean, Biochemistry 43 (2004) 1401.
[135] I. Dance, J. Am. Chem. Soc. 127 (2005) 10925.
[136] I. Dance, Inorg. Chem. 45 (2006) 5084.
[137] I. Dance, J. Am. Chem. Soc. 129 (2007) 1076.
[138] I. Dance, Chem. Asian J. 2 (2007) 936.
[139] I. Dance, Dalton Trans. (2008) 5977.
[140] I. Dance, Dalton Trans. (2008) 5992.
[141] I. Dance, Dalton Trans. 39 (2010) 2972.
[142] G.B. Seiffert, G.M. Ullmann, A. Messerschmidt, B. Schink, P.M.H. Kroneck, O. Einsle, Proc. Natl. Acad. Sci. U.S.A. 104 (2007) 3073.
[143] S. Antony, C.A. Bayse, Organometallics 28 (2009) 4938.
[144] M.A. Vincent, I.H. Hillier, G. Periyasamy, N.A. Burton, Dalton Trans. 39 (2010) 3816.
[145] K. Okamoto, Y. Kawaguchi, B.T. Eger, E.F. Pai, T. Nishino, J. Am. Chem. Soc. 132 (2010) 17080.
[146] R.-Z. Liao, J.-G. Yu, F. Himo, Proc. Natl. Acad. Sci. U.S.A. 107 (2010) 22523.